isvr Institute of Sound and Vibration Research

An Empirical Model for the Variability of the Coupling Loss Factor

W.S. Park, D.J. Thompson and N.S. Ferguson

ISVR Technical Memorandum 874

October 2001

University of Southampton

SCIENTIFIC PUBLICATIONS BY THE ISVR

Technical Reports are published to promote timely dissemination of research results by ISVR personnel. This medium permits more detailed presentation than is usually acceptable for scientific journals. Responsibility for both the content and any opinions expressed rests entirely with the author(s).

Technical Memoranda are produced to enable the early or preliminary release of information by ISVR personnel where such release is deemed to the appropriate. Information contained in these memoranda may be incomplete, or form part of a continuing programme; this should be borne in mind when using or quoting from these documents.

Contract Reports are produced to record the results of scientific work carried out for sponsors, under contract. The ISVR treats these reports as confidential to sponsors and does not make them available for general circulation. Individual sponsors may, however, authorize subsequent release of the material.

UNIVERSITY OF SOUTHAMPTON

INSTITUTE OF SOUND AND VIBRATION RESEARCH

DYNAMICS GROUP

An Empirical Model for the Variability of the Coupling Loss Factor

by

W.S. Park, D.J. Thompson and N.S. Ferguson

ISVR Technical Memorandum No: 874

October 2001

Authorised for issue by
Dr M.J.Brennan
Group Chairman

CONTENTS

1. INTRODUCTION

Statistical Energy Analysis (SEA) is based upon the power balance equation for a system which is made up of subsystems. Typically these subsystems are drawn from populations of similar members for which the ensemble average is predicted by the SEA model. Variations from the ensemble are expected for any particular realisation taken from the whole population. The coupling loss factor (CLF) is a key parameter in SEA and is defined in terms of the average behaviour of an ensemble of similar systems. However the power balance equations also hold for individual realisations, in which case the CLFs are replaced by "effective" CLFs (to distinguish them from the ensemble average CLFs). The effective CLF for a given realisation differs from the statistical average. The variability of the effective CLF has been investigated in a previous study by a numerical experiment based on a dynamic stiffness model (DSM) for a two-plate system [1]. Variations were found to depend not only on the geometric and material properties of the subsystems, such as thickness, length, width and damping, but also on frequency as the modal overlap factor increased with frequency. Results were presented in terms of the modal overlap factor of the source plate, the receiver plate, or a combination of that of both the source and receiver plates. A limitation of these results was that they were compared to the CLF derived from infinite plates, whereas a better model is available based on an ensemble average given by Wester and Mace [2]. Moreover, the use of one-third octave frequency bands, although common in practice, tended to confuse the results by making it impossible to separate the effects of frequency bandwidth and those of modal overlap. Upper and lower bounds for the CLF proposed by Craik *et al.* [3, 4] were investigated, but were found to be inappropriate to quantify the variability of the effective CLF although they are useful indicators of the degree of variability.

In this report, published models of the ensemble average [2, 5-8] are first considered to improve the estimate of the average CLF for two coupled rectangular plates. Then the variability of the effective CLF is quantified by means of a systematic parameter study. In this, the effects of frequency and modal overlap are separated by using frequency averages at a series of constant bandwidths rather than 1/3 octave band averages. These results are used to derive an empirical formula for the confidence interval of the effective CLF in terms of the modal overlap factor and the number of modes in a frequency band. This will subsequently allow confidence intervals in the SEA predictions to be determined.

2. COUPLING LOSS FACTOR

2.1 CLF from semi-infinite plates

The CLF in SEA is traditionally obtained by the travelling wave approach from semi-infinite structures [9, 10]. For two plates joined along a line this gives

$$\eta_{ij\infty} = \frac{c_{gi} b \tau_{ij}}{\pi \omega S_i} \tag{2.1}$$

where c_{gi} is the group velocity of the source subsystem i, b is the junction length, τ_{ij} is the transmission efficiency, which is the ratio of transmitted power to incident power at the boundary, and S_i is the surface area of the source subsystem. Equation (2.1) can be derived from the definition of the transmitted power and the power flow between two semi-infinite plates (see the Appendix of [1]). The transmission efficiency τ_{ij} is the angular averaged value. It is usual to assume a diffuse incident field, so that $\tau_{ij,d}$ is given by [9]

$$\tau_{ij,d} = \int_0^{\pi/2} \tau_{ij}(\theta) \cos\theta \, d\theta \tag{2.2}$$

where θ is the angle of incidence. The CLF estimates determined from the transmission efficiency for infinite subsystems, are taken as representative of ensemble averages of finite subsystems.

2.2 Ensemble average

The ensemble average CLF, based on the ensemble average response of connected rectangular plates, is given by Wester and Mace [2],

$$\eta_{ij,\,ens} = \eta_{ij\infty} \bigg/ \left[\left(\frac{1}{k_i} \int_0^{\min(k_i,k_j)} \frac{\tau_{ij}(k_y)/\tau_{ij,\,d}}{\sqrt{1+\gamma^2(k_y)}\sqrt{1+\delta^2(k_y)}} dk_y \right)^{-1} - \frac{\tau_{ij,\,d}}{\pi \mu_{i0}} \left(1 + \frac{k_i \mu_{i0}}{k_j \mu_{j0}} \right) \right] \tag{2.3}$$

where k_i and k_j are the wavenumbers of plates i and j, $\mu_{i0} = k_i l_i \eta_i / 2$ and $\mu_{j0} = k_j l_j \eta_j / 2$ are the limiting subsystem "reflectances" for small trace wavenumber k_y. $\tau_{ij}(k_y)$ corresponds to $\tau_{ij}(\theta)$ in (2.2) for $\sin\theta = k_y/k_i$. γ^2 and δ^2 are coupling parameters defined by [2]

$$\gamma^2 = \frac{\tau(k_y)\cosh^2(\mu_d)}{\sinh(\mu_i)\sinh(\mu_j)} \text{ and } \delta^2 = \frac{\tau(k_y)\sinh^2(\mu_d)}{\sinh(\mu_i)\sinh(\mu_j)} \tag{2.4}$$

where $\mu_i \approx \mu_{i0} / \sqrt{1-(k_y/k_i)^2}$, $\mu_j \approx \mu_{j0} / \sqrt{1-(k_y/k_j)^2}$ and $\mu_d = (\mu_i - \mu_j)/2$.

As an example, a two-plate system is considered with thicknesses $h_1 = 3$mm and $h_2 = 2$mm, lengths $L_1 = 0.5$m and $L_2 = 1$m, width $b = 1$m, damping $\eta_1 = \eta_2 = 0.1$ and material properties of aluminium. The ensemble average CLF $\eta_{ij,\,ens}$, the CLF for two semi-infinite plates $\eta_{ij\infty}$ and the effective CLF $\hat{\eta}_{ij}$ calculated using DSM for this two-plate system, are compared in Figure 2.1. At low frequencies, the ensemble average CLFs are lower than the semi-infinite results $\eta_{ij\infty}$ and the effective CLFs fluctuate considerably relative to $\eta_{ij,\,ens}$. These CLFs all coincide closely at high frequency where the modal overlap is high.

Figure 2.2 shows the influence of damping on the ensemble average CLF, in which the damping of the source plate, the receiver or both plates is varied. The values considered for the damping loss factors are 0.001, 0.01 and 0.1. As the damping of the source plate or the receiver increases, the ensemble average CLF increases in the low frequency region. The spread of results at low frequency indicates that approximately $\eta_{ij,\,ens} \propto \sqrt{\eta_{source}}$, and $\eta_{ij,\,ens} \propto \sqrt{\eta_{receiver}}$. A change by a factor of 100 in the individual loss factors leads to a factor of about 10 in $\eta_{ij,\,ens}$. Comparing the upper and middle graphs of Figure 2.2 it can be seen that η_{receiver} has slightly more effect than η_{source}. When both damping loss factors are equal, a change in damping loss factor causes a proportional change in $\eta_{ij,\,ens}$ at low frequency, see lower figures.

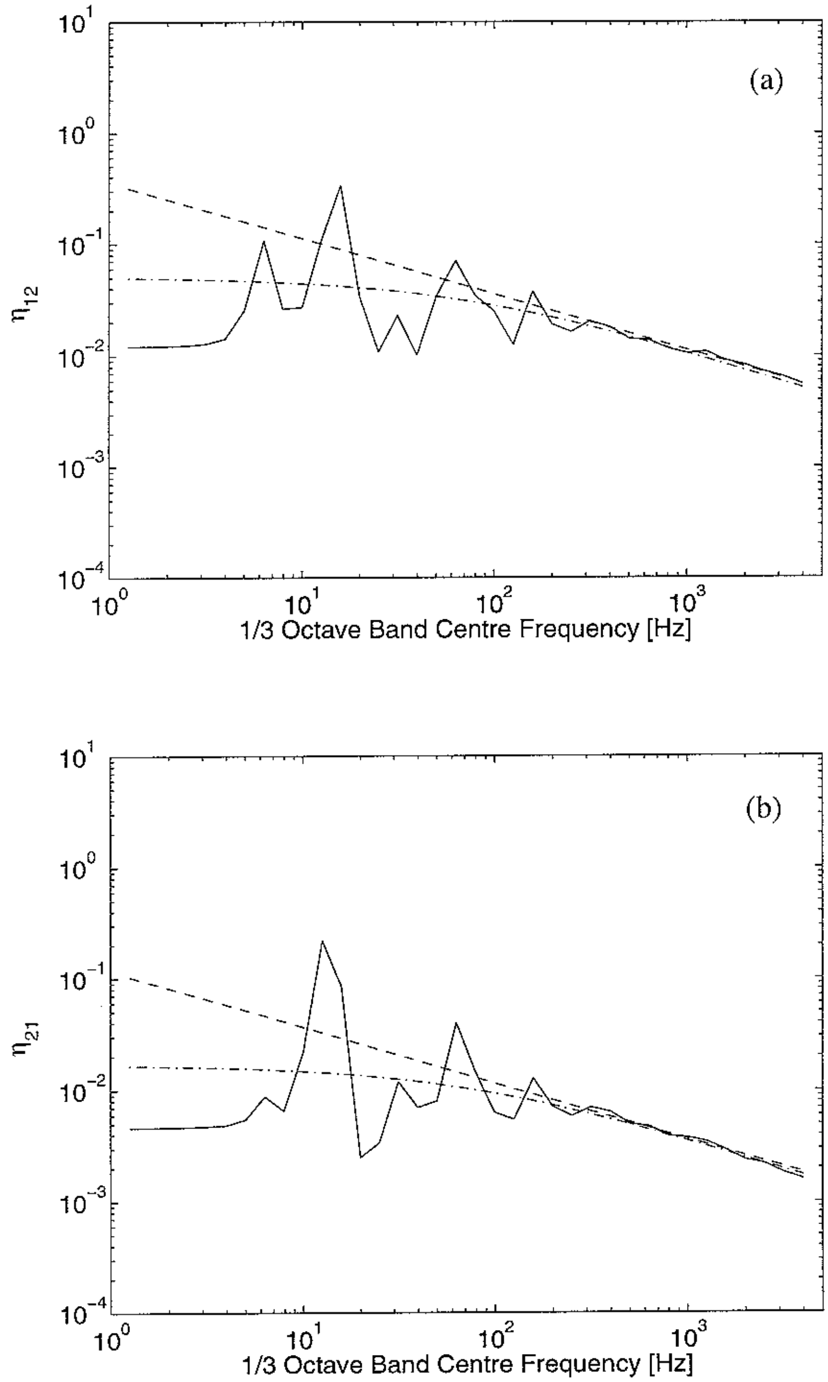

Figure 2.1. The CLFs, (a) η_{12} and (b) η_{21}, for a two-plate system (h_1 = 3mm, L_1 = 0.5m, h_2 = 2mm, L_2 = 1m, b = 1m, $\eta_1 = \eta_2 = 0.1$, material: aluminium). ---, $\eta_{ij\infty}$; -·-, $\eta_{ij,\,ens}$; —, $\hat{\eta}_{ij}$.

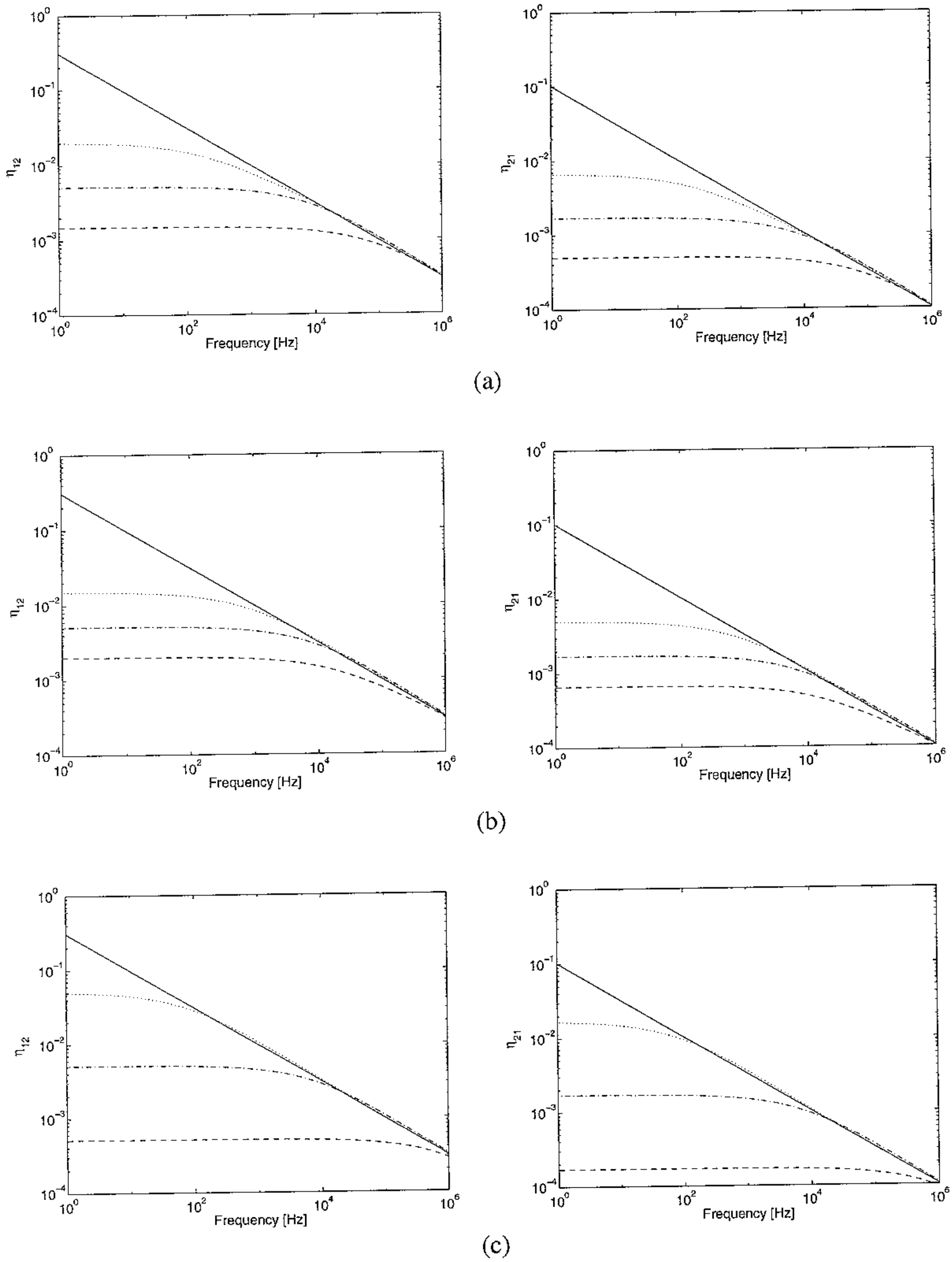

Figure 2.2. The influence of damping on the ensemble average CLF $\eta_{ij,ens}$ for the two-plate system described in Figure 2.1: (a) η_{source} is fixed as 0.01 and $\eta_{receiver}$ is varied (---, 0.001; -·-, 0.01; ·····, 0.1), (b) $\eta_{receiver}$ is fixed as 0.01 and η_{source} is varied (---,0.001; -·-, 0.01; ·····, 0.1) and (c) $\eta_{source} = \eta_{receiver}$ are varied (---, 0.001; -·-, 0.01; ·····, 0.1); —, $\eta_{ij\infty}$.

2.3 Frequency average effects on the CLF

The response of the dynamic system becomes much smoother when a frequency band average is taken. A one-third octave band average is typically used in SEA. In this study, the frequency average effects for different frequency bandwidths have been investigated. Firstly, narrow band energies and powers were calculated for the two plate system discussed above up to 1kHz using the dynamic stiffness method (DSM) at 1Hz spacing. In order to simulate a system with a constant modal overlap factor, $M = \eta\,\omega n(\omega)$, the damping loss factor has been set proportional to $1/\omega$. This gives $\eta = 0.01$ at 100Hz and 0.001 at 1kHz. Below 3Hz the damping loss factor was limited to 0.3 to avoid too high values of loss factor. The corresponding modal overlap factors are $M_1 = 0.053$ and $M_2 = 0.16$. The plate energies were then averaged over constant frequency bandwidths (20, 40, 60, 100, 200, and 400Hz) in overlapping bands. The effective CLF relating to these frequency bands $\langle \hat{\eta}_{ij} \rangle$ can be obtained from these energies by a numerical experiment as in [1]. The logarithmic ratio of the frequency averaged effective CLF to the ensemble average $10\log_{10}\left(\langle \hat{\eta}_{ij} \rangle / \eta_{ij,\,ens}\right)$ was determined, and is shown in Figure 2.3 (< > denotes a frequency averaged quantity). The mean over all centre frequencies along with a range of ±2 standard deviations (σ) is also shown. Clearly, as the bandwidth increases the range $\pm 2\sigma$ reduces, whereas the mean is close to 0 dB throughout. As the bandwidth increases, the average number of modes in a frequency band, N_1 or N_2 also increases. Figure 2.4 shows the values of 2σ from Figure 2.3 plotted against N_{12}, $= \sqrt{N_1 N_2}$, *i.e.* the geometric mean value of N_1 and N_2.

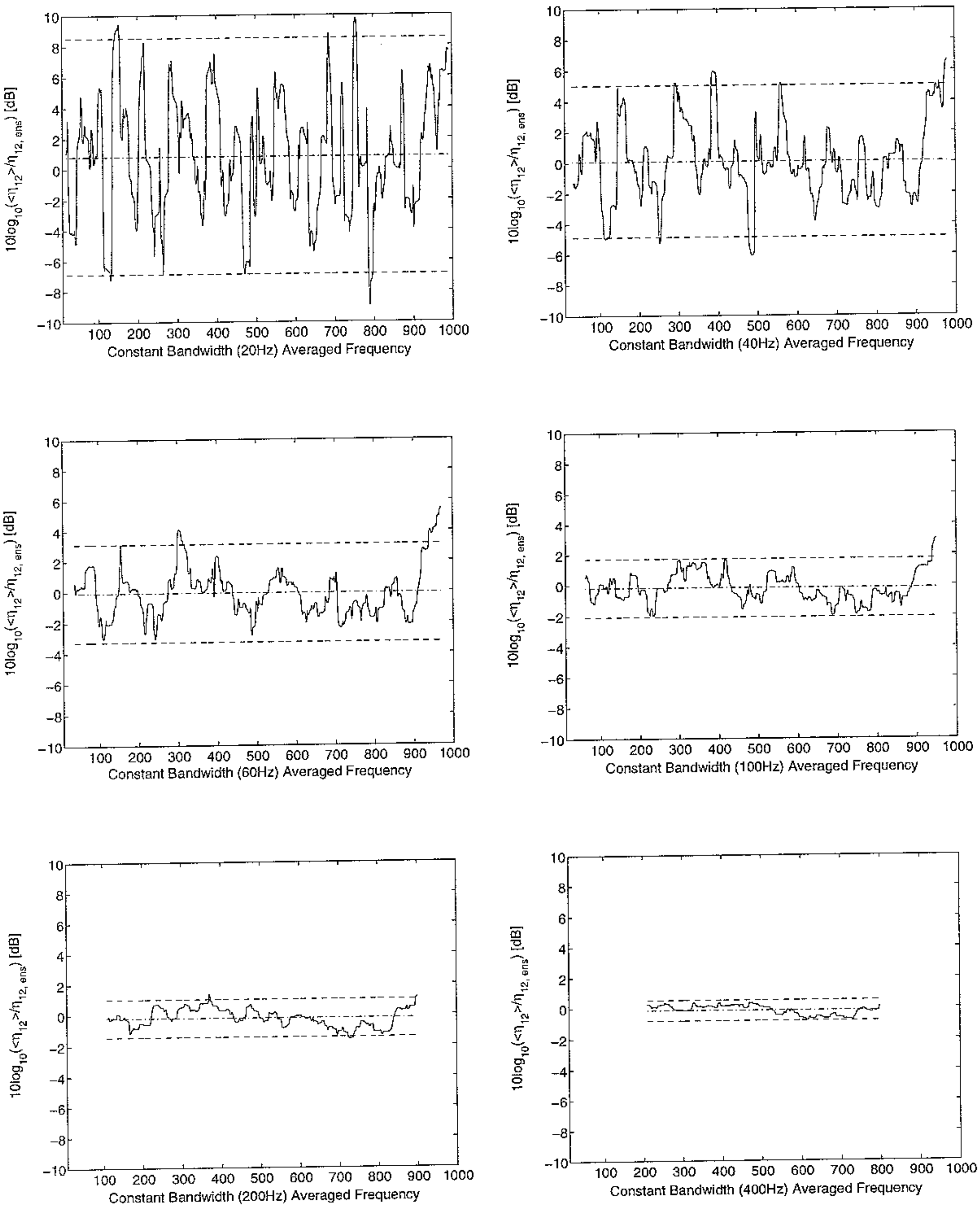

Figure 2.3. Bandwidth effect on the mean and the two standard deviation (2σ) of the logarithmic ratio of the frequency averaged effective CLF $\langle \hat{\eta}_{12} \rangle$ to the ensemble averaged CLF $\eta_{12,\,ens}$ (h_1 = 3mm, h_2 = 2mm, M_1 and M_2 fixed vs. frequency, and $\eta \propto 1/\omega$ (η = 0.3 up to 3 Hz, 0.01 at 100 Hz, and 0.001 at 1 kHz)). —, $10\log_{10}\left(\langle \hat{\eta}_{12} \rangle / \eta_{12,\,ens}\right)$; -·-, $10\log_{10}\left(\langle \hat{\eta}_{12} \rangle / \eta_{12,\,ens}\right)_{mean}$; ---, $\pm 2\sigma$ of $10\log_{10}\left(\langle \hat{\eta}_{12} \rangle / \eta_{12,\,ens}\right)_{mean}$.

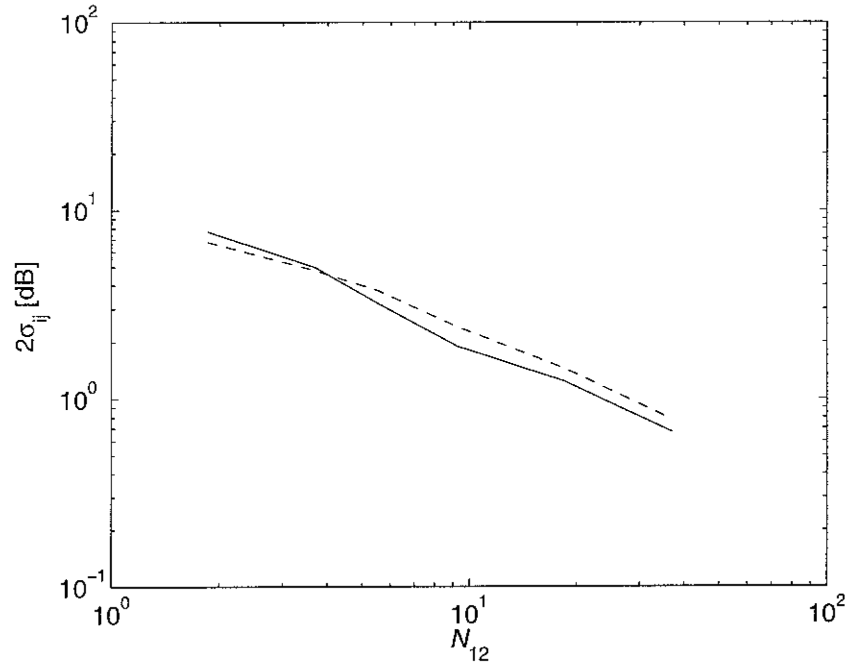

Figure 2.4. Two standard deviations (2σ) of the logarithmic ratio of the frequency averaged effective CLF to the ensemble averaged CLF, $10\log_{10}\left(\left\langle\hat{\eta}_{ij}\right\rangle/\eta_{ij,\,ens}\right)$ (h_1 = 3mm, h_2 = 2mm, M_1 and M_2 fixed vs. frequency, and $\eta \propto 1/\omega$ (η = 0.3 up to 3Hz, 0.01 at 100Hz, and 0.001 at 1kHz)): —, $2\sigma_{12}$; ---, $2\sigma_{21}$.

2.4 Review of previous DSM results

A sensitivity analysis has been performed [1] using the DSM model to evaluate the influence of the following parameters: the plate thickness ratio, h_1/h_2, the length ratio, L_1/L_2, the length to width ratio of the two plates L_1/b and the damping loss factors, $\eta_1 = \eta_2$. In the calculations, the dimensions of plate 1 (L_1 = 0.5 m, b = 1 m, h_1 = 3 mm) were kept fixed and the relevant dimensions of plate 2 were given 11 logarithmically spaced values between 0.3 and 3 times that for plate 1. The values considered for the damping loss factor were 0.03, 0.1 and 0.3.

Two issues were investigated; one was the validity of Craik's upper and lower bounds for the CLF [3] and the other was to determine whether the variability in the CLF depends on the modal properties of the source subsystem, the receiver subsystem, or both the source and receiver subsystems. It appeared, from the results presented, that Craik's upper and lower bounds are a useful indication of variability in the CLF, although better agreement occurs when the modal overlap of both subsystems is taken into account, rather than that of the receiver as originally proposed by Craik [3]. However these bounds did not account for remaining variability when the modal overlap is greater than about 0.5. In a further study [11], the variability in the CLF has been examined in more detail using a model of a finite source plate coupled to an infinite receiver and vice versa. Large variability in the energy transmission was found due to the modal behaviour of the receiver plate, with peaks occurring in the transmission efficiency at the receiver's resonances. Damping of the receiver plate controlled the magnitude of these variations. However, smaller variations in the energy transmission were attributed to the source subsystem characteristics, as produced using the finite source plate coupled to a semi-infinite receiver plate. Both peaks and troughs in the effective CLF corresponded to natural frequencies of the uncoupled source plate, but damping of the source plate had only a small influence. Therefore it has been suggested that the modal overlap of the receiver plate is important whereas the modal density (not its damping) of the source plate is important.

In order to resolve these questions a further procedure to investigate the dependence of the variability on the various parameters has been conducted and is described in the remainder of this report.

3. PARAMETER VARIATION USING THE DSM MODEL

The variability of the effective CLF was investigated in the previous study by a numerical experiment based on a dynamic stiffness model for a two-plate system [1]. The CLF was found to depend not only on the geometric and material properties of the subsystems, such as thickness, length, width and damping, but also on frequency as the modal overlap factor increased with frequency. Results were presented in terms of the modal overlap factor of the source plate, the receiver plate, or a combination of that of both the source and receiver plates. The previous calculations did not consider the ensemble average [2, 5-8]. Moreover, the frequency, the bandwidth, and the modal overlap factor were not varied independently.

In this study, the modal density $n(\omega)$ and modal overlap factor M, which affect the variability of the CLF, are considered as independent control parameters. The ensemble average is also used as the reference for studying variability. The purpose is to express the variability of the CLF in terms of an empirical formula. This should then allow confidence intervals in SEA predictions to be obtained.

The modal density and modal overlap factor are related to the geometric and material properties. The modal density of a simply supported uniform isotropic plate is approximated as

$$n(\omega) = \left(\frac{S}{4\pi}\right)\left(\frac{\rho h}{D}\right)^{1/2} \tag{3.1}$$

where S is the area of plate, ρ is the material density, h is the thickness of plate and $D\left(=\dfrac{Eh^3}{12(1-\nu^2)}\right)$ is the flexural rigidity [12]. If the material properties are assumed to be constant, the modal density is proportional to the *area* (*length* $\times$ *width*) / *thickness* of plate and it is independent of frequency. The number of modes in a frequency band of width $\Delta\omega$ is

$$N = \Delta\omega n(\omega) \tag{3.2}$$

On the other hand, the modal overlap factor is given by

$$M = \eta\,\omega n(\omega) \tag{3.3}$$

where η is the damping loss factor. Thus the modal overlap factor is in general dependent on frequency as well as the geometric and material properties.

The effective CLF and the ensemble average CLF described in Chapter 2 are individually investigated by varying these parameters as well as varying the geometric parameters considered in the previous study for an L-shaped coupled plate system [1]. First, a coupled aluminium plate model (length $L_1 = 0.5$m and $L_2 = 1.0$m, thickness $h_1 = 3$mm and $h_2 = 2$mm, and width $b = 1.0$m) is considered, as a baseline model, see section 2.2. This model has a modal density that is constant with varying frequency but the modal overlap factor depends on frequency. Then, in order to keep the modal overlap factors M_1 and M_2 fixed, the damping loss factor is chosen to vary *i.e.* $\eta \propto 1/\omega$. The damping loss factors of the two plates are assumed to be equal, and three different levels of damping loss factor (0.1, 0.03 and 0.01 at 100 Hz) are considered to investigate the effect of damping. In this case, as $\eta_1 = \eta_2$, $M_2N_1/M_1N_2 = 1.0$. These results are intended to show the effective CLF and its variability due to frequency bandwidth and different levels of damping.

To investigate the effect of different damping for the two plates, whilst keeping the modal overlap factors constant, calculations also performed with the damping loss factors for the two plates chosen to have different levels of damping while retaining $\eta \propto 1/\omega$. These were high to medium ($M_2N_1/M_1N_2 = 0.3$) and medium to low ($M_2N_1/M_1N_2 = 0.33$).

Next, a series of systematic numerical simulations are performed covering extensive parameter variations similar to those described in [1]. The influence of these parameters on the variability of the CLF is investigated by keeping the dimension of plate 1 fixed and giving the dimension of plate 2 logarithmically spaced values. The modal densities of the two plates are kept constant for each calculation. The damping values of the two plates are varied with frequency $\eta \propto 1/\omega$, in order to keep the modal overlap factors fixed, as before. The other parameters are the same as the baseline model.

The parameters used in this study are summarised in Table 3.1 and the values of plate thickness ratio h_1/h_2, the length ratio L_1/L_2, and the length to width ratio L_1/b of the two plates, are shown below the table. The values of parameters will be given in detail in the following chapter along with the results.

Table 3.1. Parameter variations for L-shaped coupled plates.

Parameter	Fixed	Varied	M_1	M_2	M_2N_1/M_1N_2
Baseline (h_1=3mm h_2=2mm)	$L_1,L_2,h_1,h_2,b,\eta_1,\eta_2,n_1(\omega),n_2(\omega)$	M_1, M_2			1.0
High damping	L_1,L_2,h_1,h_2,b	$\eta_1=\eta_2\propto 1/\omega$	0.53	1.6	1.0
Medium damping	L_1,L_2,h_1,h_2,b	$\eta_1=\eta_2\propto 1/\omega$	0.16	0.48	1.0
Light damping	L_1,L_2,h_1,h_2,b	$\eta_1=\eta_2\propto 1/\omega$	0.053	0.16	1.0
$\eta_1>\eta_2$	L_1,L_2,h_1,h_2,b	$\eta_1\neq\eta_2\propto 1/\omega$	0.53	0.48	0.30
$\eta_1>\eta_2$	L_1,L_2,h_1,h_2,b	$\eta_1\neq\eta_2\propto 1/\omega$	0.16	0.16	0.33
h_1/h_2 (*1)	L_1,h_1,b	L_2,h_2,η_1,η_2	0.53	1.6	1.0
L_1/L_2 (*2)	L_1,h_1,h_2,b	L_2,η_1,η_2	0.53	2.5~0.32	1.0
L_1/b (*3)	h_1,h_2	L_1,L_2,b,η_1,η_2	0.53	1.6	1.0

(*1) h_1/h_2: the thickness of plate 1 (3mm) is fixed and the thickness of plate 2 is varied from 9.49mm to 0.949mm (9.49, 5.99, 4.75, 3.78, 3.00, 2.38, 1.89, 1.50,1.19, 0.949mm). The length L_2 is varied simultaneously to ensure constant N_2.

(*2) L_1/L_2: the length of plate 1 (0.5m) is fixed and the length of plate 2 is varied from 1.58m to 0.20m (1.58, 1.26, 1.00, 0.79, 0.63, 0.50, 0.40, 0.32, 0.25, 0.20m).

(*3) L_1/b: the widths of the two plates are varied from 1.58m to 0.20m (1.58, 1.26, 1.00, 0.79, 0.63, 0.50, 0.40, 0.32, 0.25, 0.20m). The lengths of the plates are varied simultaneously to maintain the same areas and hence constant values of N_1 and N_2. The variation of η_1 and η_2 subsequently produces constant values of M_1 and M_2.

4. THE VARIABILITY OF THE CLF

4.1 Baseline model

4.1.1 Modal density fixed with varying modal overlap factor

The effective CLF $\hat{\eta}_{ij}$, the ensemble averaged CLF $\eta_{ij,\,ens}$, and the CLF for semi-infinite plates $\eta_{ij\infty}$ for the baseline model, with the modal densities fixed as described in the previous chapter, have been shown in Figure 2.1. The results were averaged over 1/3 octave frequency bands as typically used in SEA. The effective CLFs fluctuated considerably relative to $\eta_{ij,\,ens}$ or $\eta_{ij\infty}$ and these CLFs all coincided more closely as frequency increased.

In the remainder of the results, constant bandwidth frequency averaging is used and the damping is adjusted to make the modal overlap factor independent of frequency.

4.1.2 Modal overlap factor fixed without varying modal density (η_1=η_2)

In order to achieve a fixed modal overlap factor for all frequencies without varying the modal density, the damping was chosen as inversely proportional to frequency, $\eta_1 = \eta_2 \propto 1/\omega$. Three levels of damping (characterised by $\eta = 10/f$, $3/f$ and $1/f$ with f the frequency) were considered to investigate the influence of the modal overlap factor on the CLF. The maximum damping was limited to 0.3 at low frequencies to avoid numerical difficulties. Since $\eta_1 = \eta_2$, the ratio M_2N_1/M_1N_2 with M the modal overlap factor and N the number of modes in a frequency band for the three levels of damping was fixed as 1. Figure 4.1 shows the effective CLFs and the ensemble averaged CLF calculated at 1Hz spacing up to 1kHz. Also shown, are the estimates of upper and lower bounds, $2/\pi M$ and $\pi M/2$, obtained from the maxima and minima of the mobility given by Skudrzyk [13] and used in a formula for CLF similar to that given by Craik *et al.* [3, 4]. These bounds were based on using the modal overlap factor for the source plate M_s, the receiver plate M_r, and the geometric mean values $\sqrt{M_s M_r}$. It can be seen that the variation in the CLF is considerably greater than that estimated from the bounds shown.

These effective CLFs were next determined using energies averaged over frequency bands with bandwidths of 2, 4, 6, 10, 20, 40, 60, 100, 200 and 400Hz in overlapping bands, as described in section 2.2. Then the logarithmic ratio of the effective CLF to the ensemble average, $10\log_{10}\left(\langle\hat{\eta}_{ij}\rangle/\eta_{ij,\,ens}\right)$, was determined as in Figure 2.3. The range of two standard deviations (2σ) was obtained over the whole frequency region to express the variability of the effective CLF compared to the ensemble average. Figure 4.2 shows the values of 2σ plotted against N_{12}, which is the geometric mean value of the number of modes per band for the two plates. This shows that the variability of the effective CLF depends upon the number of the modes per frequency band when this number is larger than about 1, whereas it depends on the damping (modal overlap factor) when there are few modes in a band. The uncertainty (2σ)

increases as the average number of modes in a band reduces to about 1. Below this it reaches a value that is independent of any further change in the frequency bandwidth. The value of 2σ at low values of N_{12} increases as the damping reduces (*i.e.* M_1 and M_2 reduce). Interestingly, the results for η_{12} and η_{21} are similar despite the values of M differing by a factor of 3.

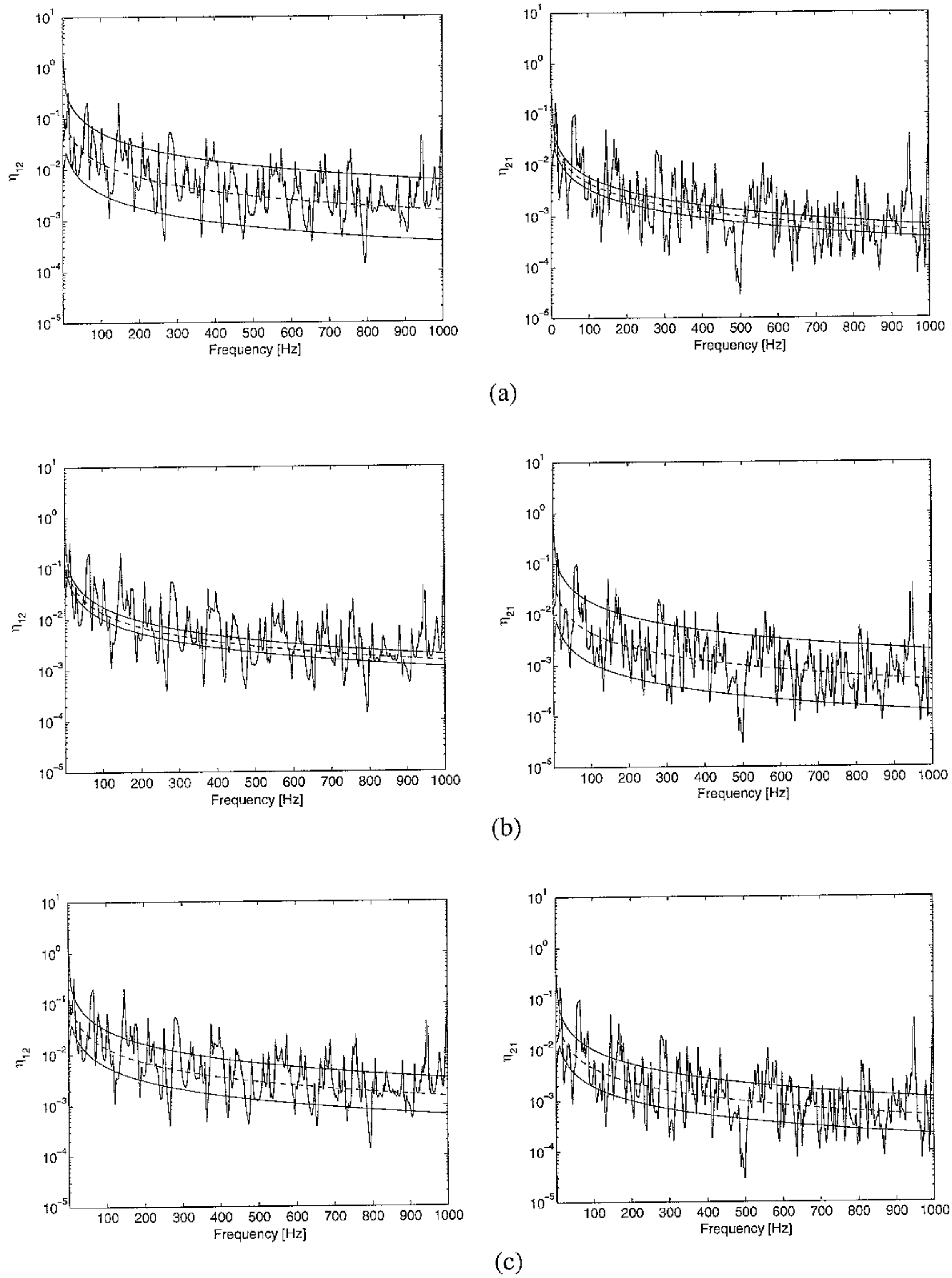

Figure 4.1. The CLFs for the medium damping values ($\eta = \min(0.3,\ 10/f)$, $M_1 = 0.16$, $M_2 = 0.48$ fixed, $M_2N_1/M_1N_2 = 1.0$). —, the effective CLF; -·-, the ensemble averaged CLF; ---, upper and lower bounds derived from Skudrzyk bounds for mobility [13]; (a) M_s, (b) M_r, and (c) $\sqrt{M_s M_r}$.

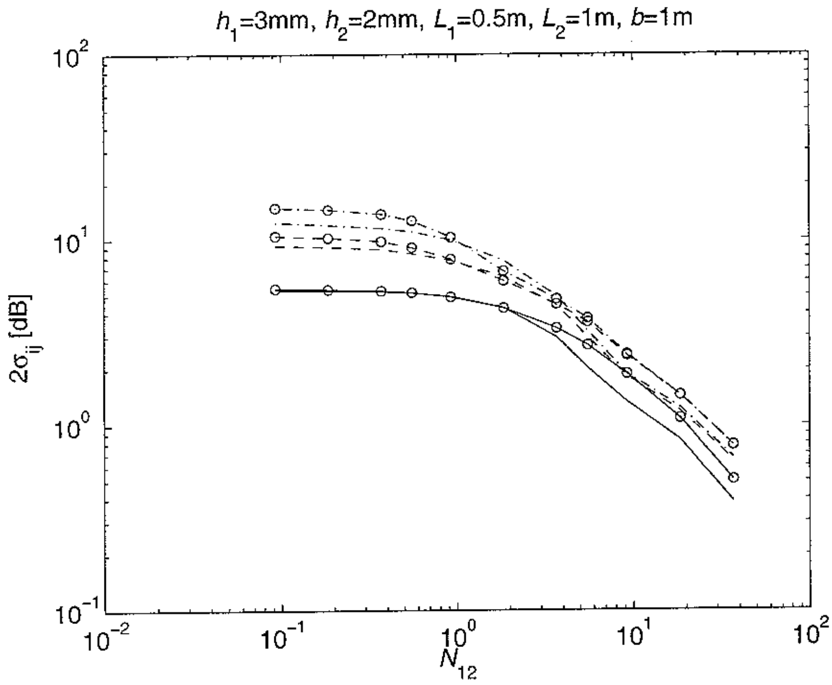

Figure 4.2. Variability of the CLF (2σ) for 3 levels of damping $\eta_1 = \eta_2$ as a function of N_{12} as bandwidth is altered. —, $M_1 = 0.53$, $M_2 = 1.6$; ---, $M_1 = 0.16$, $M_2 = 0.48$; -·-, $M_1 = 0.05$, $M_2 = 0.16$. Circles denote 2σ for η_{21}.

4.1.3 Modal overlap factor and modal density ratio (M_2N_1/M_1N_2) fixed ($\eta_1 \neq \eta_2$)

Using different damping values for the two plates whilst keeping the modal overlap factors constant with frequency, the ratio M_2N_1/M_1N_2 takes values other than 1. Three damping values (high damping = $10/f$, medium damping = $3/f$ and low damping = $1/f$), were combined to give different damping values for the two plates: high to medium and medium to low. The maximum damping was again limited to 0.3 at low frequencies as described in the previous section. Figure 4.3 shows the variability (2σ) of the logarithmic ratio of the effective CLF to the ensemble average, $10\log_{10}\left(\left\langle \hat{\eta}_{ij} \right\rangle / \eta_{ij,\,ens}\right)$, as a function of N_{12} for these cases. Similar trends are found to those in Figure 4.2. Again the results for η_{12} and η_{21} are similar in each case despite differences in the damping of the two plates.

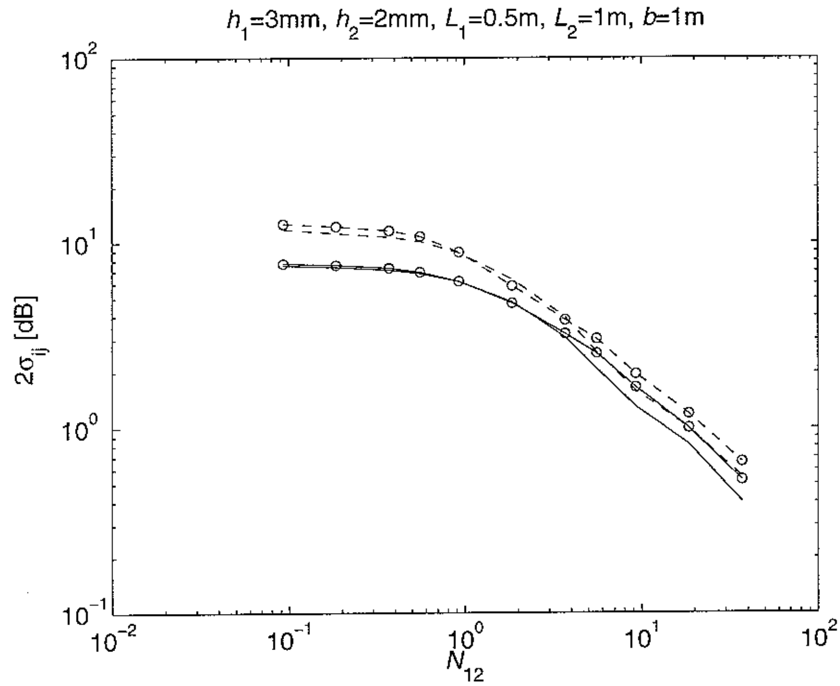

Figure 4.3. Variability of the CLF (2σ) as a function of N_{12} as bandwidth is altered. Modal overlap factor constant for all frequencies, $\eta_1 \neq \eta_2$. —, $\eta_1 = 10/f$, $\eta_2 = 3/f$, $M_2N_1/M_1N_2 = 0.3$; ---, $\eta_1 = 3/f$, $\eta_2 = 1/f$, $M_2N_1/M_1N_2 = 0.33$. Circles denote 2σ for η_{21}.

4.2 The variation of thickness ratio (h_1/h_2): constant modal overlap factors without varying modal density

To investigate the influence of the plate thickness ratio h_1/h_2 on the variability of the CLF, the thickness of plate 1 was kept fixed and the thickness of plate 2 was given 11 logarithmically spaced values between 0.32 and 3.2 times that for plate 1 as listed in Table 4.1. In order to retain the same value for the modal density of plate 2, its length was varied to compensate for the thickness, see equation (3.1). The damping values of the two plates were varied with frequency in order to give constant values of the modal overlap factor, as before. The other parameters were the same as the baseline model. The effective CLF and the ensemble average CLF for the 11 cases were calculated and their logarithmic ratio, $10\log_{10}\left(\hat{\eta}_{ij}/\eta_{ij,ens}\right)$, in dB is shown in Figure 4.5 derived from results at 1Hz spacing up to 1kHz. The results below 1.25 times the lower of the cut-on frequencies of the two plates were excluded, as SEA assumptions would not be valid and it is inappropriate to use an SEA approach. All of the results fall within ±10dB.

These results were also determined using energies averaged over frequency bands (2, 4, 6, 10, 20, 40, 60, 100, 200, and 400Hz) in overlapping bands. The two standard deviation range (2σ) of $10\log_{10}\left(\left\langle \hat{\eta}_{ij} \right\rangle / \eta_{ij,\,ens}\right)$ was calculated in each case and a graph of 2σ against N_{12} is shown in Figure 4.6. The variability of the effective CLF is affected slightly by the plate thickness ratio h_1/h_2 but much more by the frequency bandwidth. The dependence on the number of modes in the band N_{12} has a similar form to those shown in Figure 4.2 and 4.3. The results seem to be highest for either large or small values of h_1/h_2; the results are lowest for $h_1/h_2 \cong 1$.

Table 4.1. Parameter variations of the plate thickness ratio h_1/h_2 for 11 variants

Parameter	h_1 (mm)	h_2 (mm)	L_1 (m)	L_2 (m)	b (m)	$n_1(\omega)$	$n_2(\omega)$	M_1	M_2
1	3.00	9.49	0.50	4.74	1.00	0.009	0.026	0.53	1.60
2	3.00	7.54	0.50	3.77	1.00	0.009	0.026	0.53	1.60
3	3.00	5.99	0.50	2.99	1.00	0.009	0.026	0.53	1.60
4	3.00	4.75	0.50	2.37	1.00	0.009	0.026	0.53	1.60
5	3.00	3.78	0.50	1.89	1.00	0.009	0.026	0.53	1.60
6	3.00	3.00	0.50	1.50	1.00	0.009	0.026	0.53	1.60
7	3.00	2.38	0.50	1.19	1.00	0.009	0.026	0.53	1.60
8	3.00	1.89	0.50	0.944	1.00	0.009	0.026	0.53	1.60
9	3.00	1.50	0.50	0.749	1.00	0.009	0.026	0.53	1.60
10	3.00	1.19	0.50	0.594	1.00	0.009	0.026	0.53	1.60
11	3.00	0.949	0.50	0.474	1.00	0.009	0.026	0.53	1.60

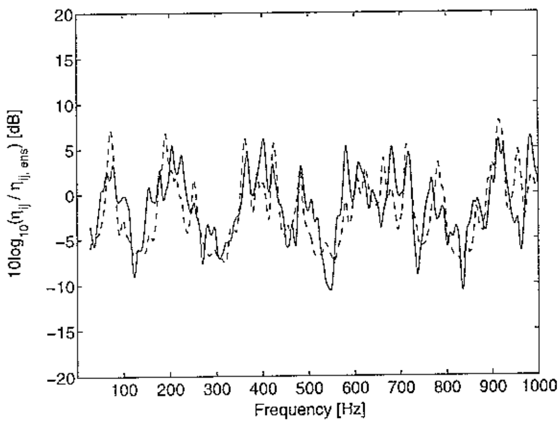

(a) h_2 = 9.49mm, L_2 = 4.74m

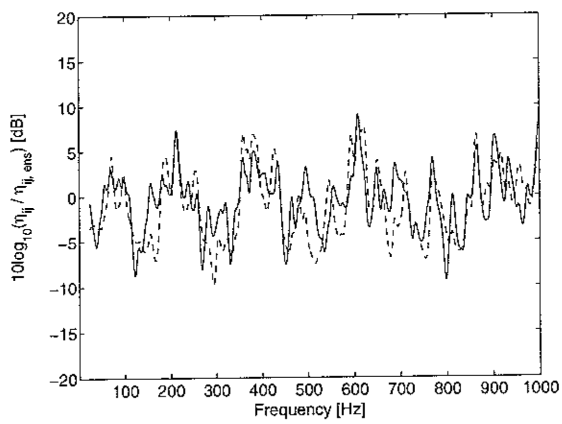

(b) h_2 = 7.54mm, L_2 = 3.77m

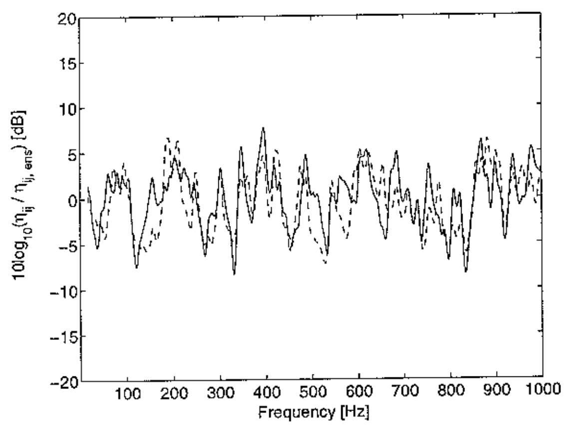

(c) h_2 = 5.99mm, L_2 = 2.99m

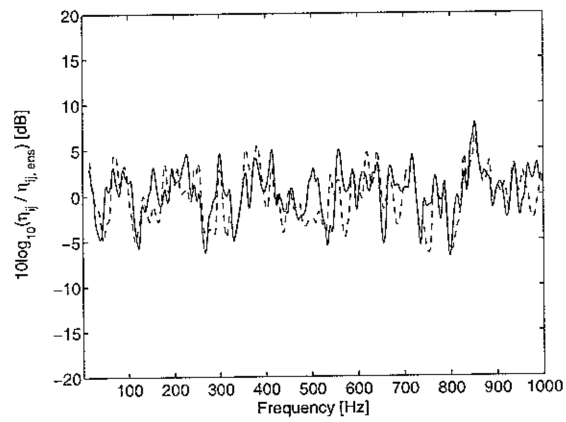

(d) h_2 = 4.75mm, L_2 = 2.37m

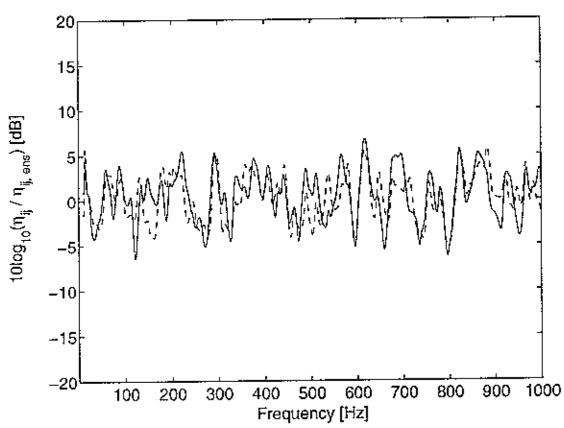

(e) h_2 = 3.78mm, L_2 = 1.89m

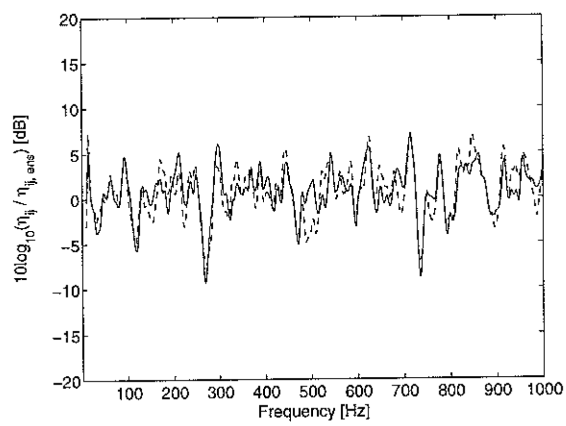

(f) h_2 = 3.00mm, L_2 = 1.50m

Figure 4.5 (a)-(f). The logarithmic CLF ratio $10\log_{10}\left(\hat{\eta}_{ij}/\eta_{ij,\,ens}\right)$ for different values of h_1/h_2 with constant modal overlap factors, M_1 = 0.53 and M_2 = 1.6 (h_2 and L_2 are varied, η depends on frequency). —, $10\log_{10}\left(\hat{\eta}_{12}/\eta_{12,\,ens}\right)$; ---, $10\log_{10}\left(\hat{\eta}_{21}/\eta_{21,\,ens}\right)$.

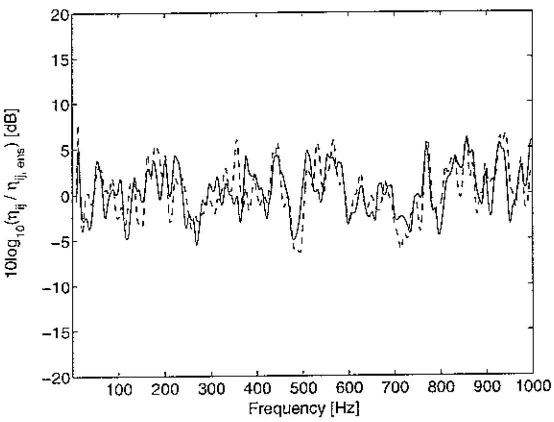

(g) $h_2 = 2.38$mm, $L_2 = 1.19$m

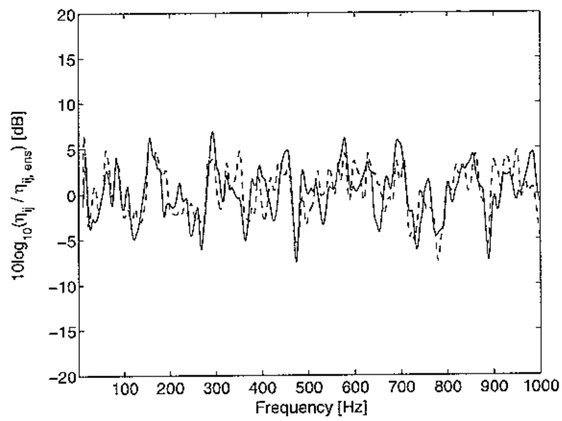

(h) $h_2 = 1.89$mm, $L_2 = 0.94$m

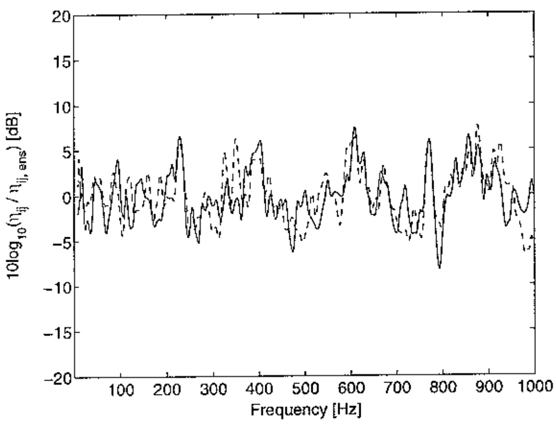

(i) $h_2 = 1.50$mm, $L_2 = 0.75$m

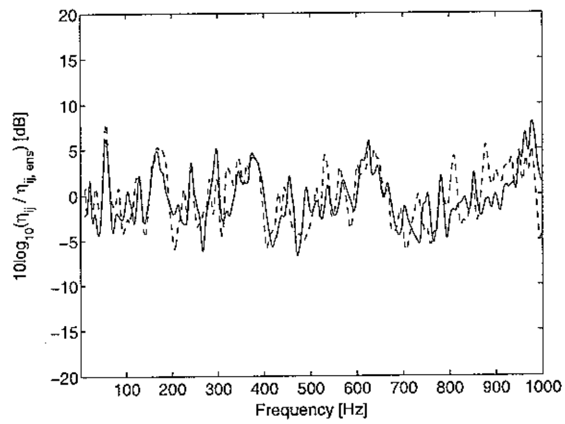

(j) $h_2 = 1.19$mm, $L_2 = 0.59$m

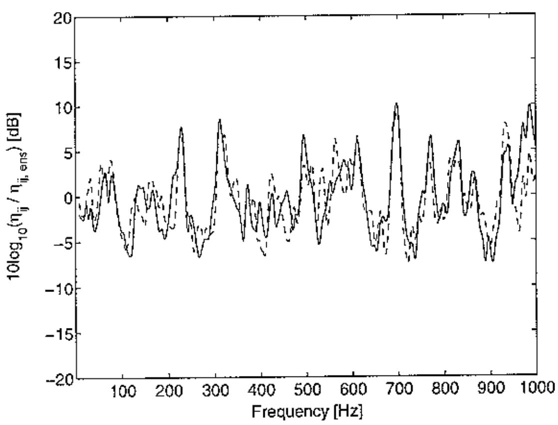

(k) $h_2 = 0.95$mm, $L_2 = 0.47$m

Figure 4.5 (g)-(k). The logarithmic CLF ratio $10\log_{10}\left(\hat{\eta}_{ij}/\eta_{ij,\,ens}\right)$ for different values of h_1/h_2 with constant modal overlap factors, $M_1 = 0.53$ and $M_2 = 1.6$ (h_2 and L_2 are varied, η depends on frequency). —, $10\log_{10}\left(\hat{\eta}_{12}/\eta_{12,\,ens}\right)$; ---, $10\log_{10}\left(\hat{\eta}_{21}/\eta_{21,\,ens}\right)$.

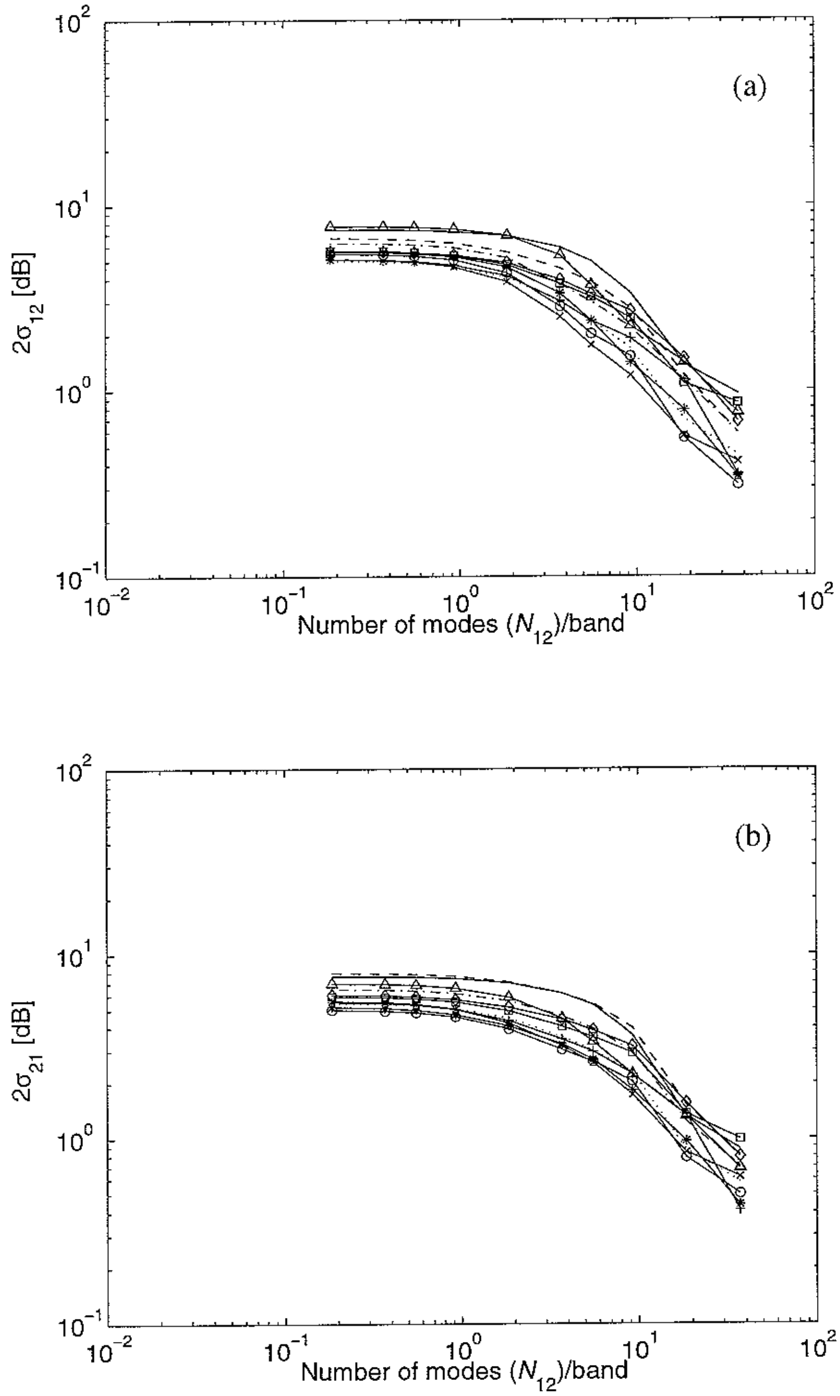

Figure 4.6. Variability of the CLF (2σ), (a) σ_{12} and (b) σ_{21}, for different values of h_1/h_2 with constant modal overlap factors, $M_1 = 0.53$ and $M_2 = 1.6$ (h_2 and L_2 are varied, η depends on frequency). —, 9.49; ---, 7.54; -·-, 5.99; ····, 4.75; -o-, 3.78; -×-, 3.00; -+-, 2.38; -*-, 1.89; -□-, 1.50; -◇-,1.19; -△-, 0.95 (h_2 in millimetres).

4.3 The variation of length ratio (L_1/L_2): varying modal overlap factor ratio

The influence of the plate length ratio L_1/L_2 on the variability of the CLF was investigated by keeping the length of plate 1 fixed and giving the length of plate 2 each of 10 logarithmically spaced values between 0.4 and 3.16 times that for plate 1 as listed in Table 4.2. The damping was again chosen to be inversely proportional to frequency so that the modal overlap factor for each plate was constant. The modal overlap factor for plate 2 was constant for each calculation, but was proportional to its length. The other parameters were the same as the baseline model. The effective CLF and the ensemble average CLF for the 10 cases were calculated and the logarithmic ratio of the effective CLF to the ensemble average $10\log_{10}\left(\hat{\eta}_{ij}/\eta_{ij,\,ens}\right)$ in dB is shown in Figure 4.7, for results calculated at 1Hz spacing up to 1kHz. The results below 1.25 times the lower of the first cut-on frequencies of the two plates were excluded, as in the previous section. All of the results fall within ±10dB except for $L_2 = 0.4$m where a single peak of 30dB is seen.

The results were next determined using energies averaged over frequency bands (2, 4, 6, 10, 20, 40, 60, 100, 200, and 400Hz) in overlapping bands. The two standard deviation range (2σ) of $10\log_{10}\left(\langle\hat{\eta}_{ij}\rangle/\eta_{ij,\,ens}\right)$ was calculated and is shown plotted against N_{12} in Figure 4.8. These results show that the variability of the effective CLFs depend somewhat on the ratio of M_1 to M_2, introduced here by varying the plate length ratio L_1/L_2. The constant value of 2σ for low N_{12} is greatest when $M_1/M_2 \cong 1$ (* in Figure 4.8) and lowest when M_1 and M_2 are most dissimilar. The result for $L_2 = 0.4$m does not show up as unusual when averaged over the whole frequency range.

Table 4.2. Parameter variations of the plate length ratio L_1/L_2 for 10 variants

Parameter	h_1 (mm)	h_2 (mm)	L_1 (m)	L_2 (m)	b (m)	$n_1(\omega)$	$n_2(\omega)$	M_1	M_2
1	3.00	2.00	0.50	1.58	1.00	0.009	0.040	0.53	2.53
2	3.00	2.00	0.50	1.26	1.00	0.009	0.032	0.53	2.02
3	3.00	2.00	0.50	1.00	1.00	0.009	0.026	0.53	1.60
4	3.00	2.00	0.50	0.79	1.00	0.009	0.020	0.53	1.26
5	3.00	2.00	0.50	0.63	1.00	0.009	0.016	0.53	1.01
6	3.00	2.00	0.50	0.50	1.00	0.009	0.013	0.53	0.80
7	3.00	2.00	0.50	0.40	1.00	0.009	0.010	0.53	0.64
8	3.00	2.00	0.50	0.32	1.00	0.009	0.008	0.53	0.51
9	3.00	2.00	0.50	0.25	1.00	0.009	0.006	0.53	0.40
10	3.00	2.00	0.50	0.20	1.00	0.009	0.005	0.53	0.32

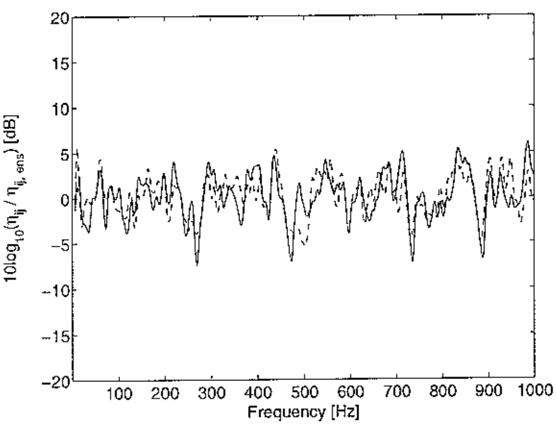

(a) $L_2 = 1.58\text{m}, M_1/M_2 = 0.21$

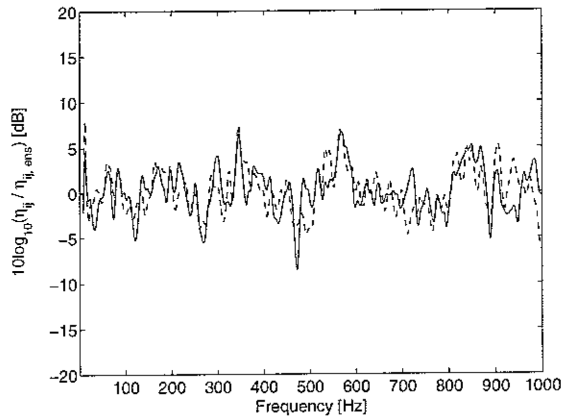

(b) $L_2 = 1.26\text{m}, M_1/M_2 = 0.26$

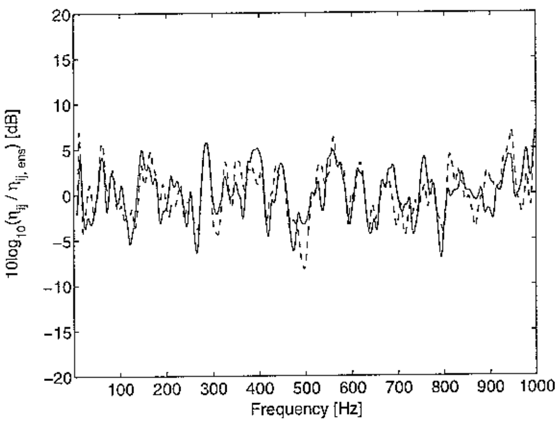

(c) $L_2 = 1.00\text{m}, M_1/M_2 = 0.33$

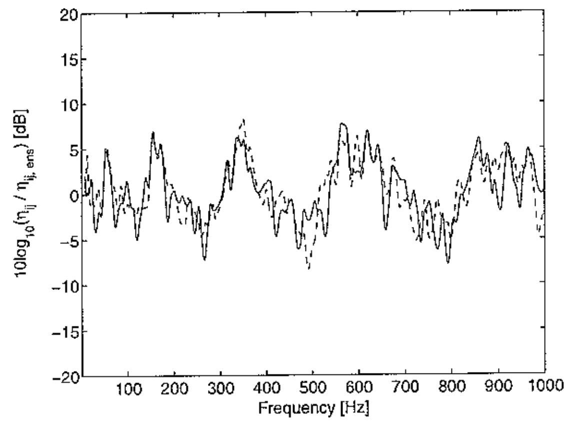

(d) $L_2 = 0.79\text{m}, M_1/M_2 = 0.42$

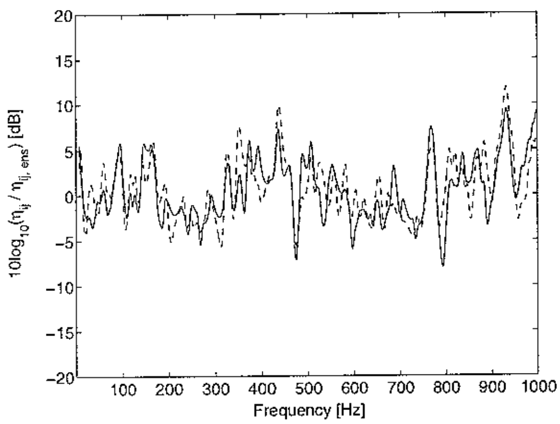

(e) $L_2 = 0.63\text{m}, M_1/M_2 = 0.53$

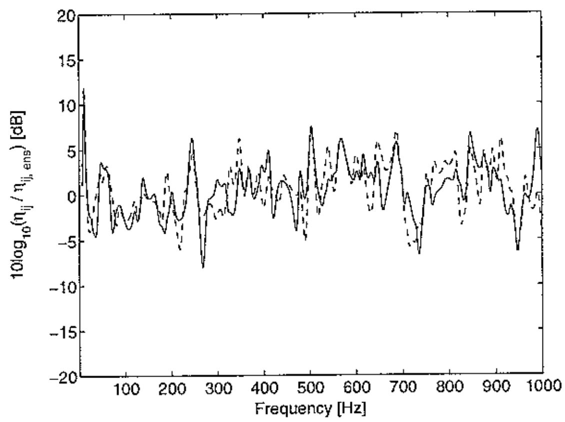

(f) $L_2 = 0.50\text{m}, M_1/M_2 = 0.67$

Figure 4.7 (a)-(f). The logarithmic CLF ratio $10\log_{10}\left(\hat{\eta}_{ij}/\eta_{ij,\,ens}\right)$ for different values of L_1/L_2. The modal overlap factor ratio M_1/M_2 varies between 0.21 and 1.66 ($M_1 = 0.53$ is fixed, L_2 and M_2 (= 2.53 ~ 0.32) varying). —, $10\log_{10}\left(\hat{\eta}_{12}/\eta_{12,\,ens}\right)$; ---, $10\log_{10}\left(\hat{\eta}_{21}/\eta_{21,\,ens}\right)$.

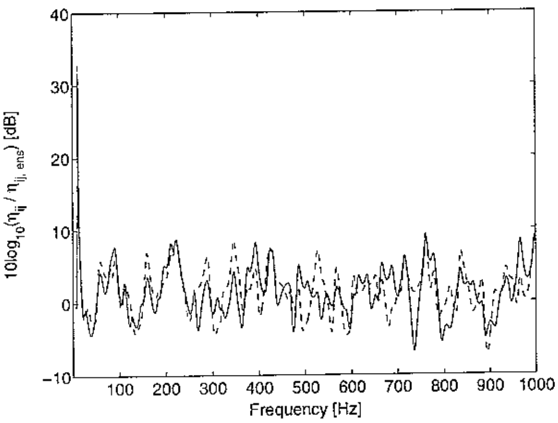

(g) $L_2 = 0.40\text{m}$, $M_1/M_2 = 0.83$

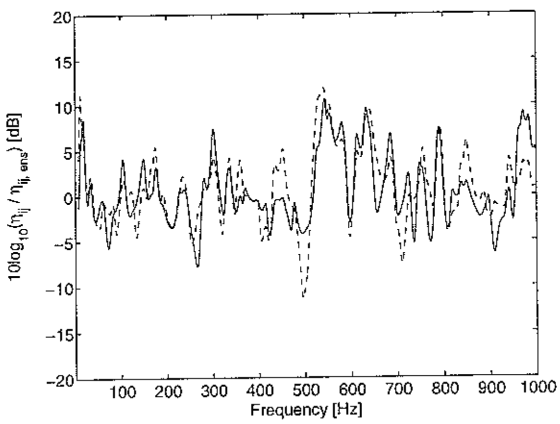

(h) $L_2 = 0.32\text{m}$, $M_1/M_2 = 1.04$

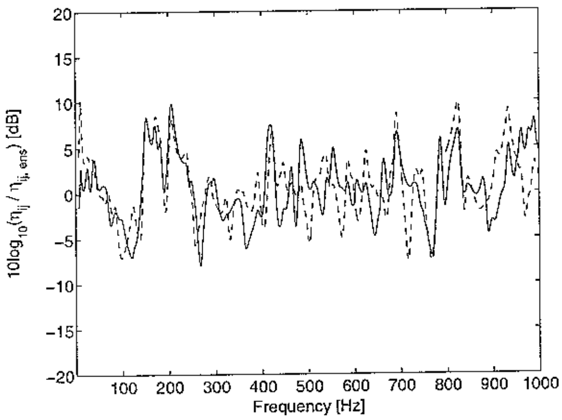

(i) $L_2 = 0.25\text{m}$, $M_1/M_2 = 1.33$

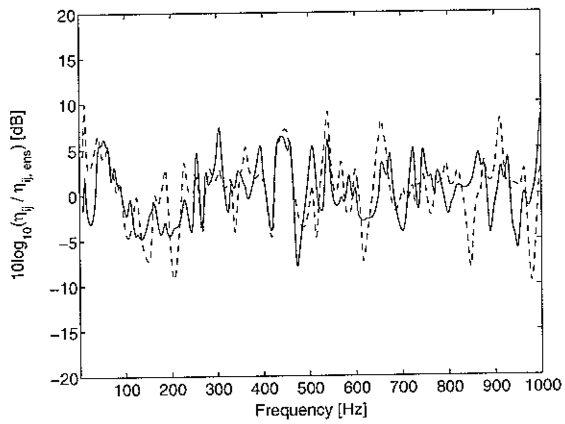

(j) $L_2 = 0.20\text{m}$, $M_1/M_2 = 1.67$

Figure 4.7 (g)-(j). The logarithmic CLF ratio $10\log_{10}\left(\hat{\eta}_{ij}/\eta_{ij,\,ens}\right)$ for different values of L_1/L_2. The modal overlap factor ratio M_1/M_2 varies between 0.21 and 1.66 ($M_1 = 0.53$ is fixed, L_2 and M_2 (= 2.53 ~ 0.32) varying). —, $10\log_{10}\left(\hat{\eta}_{12}/\eta_{12,\,ens}\right)$; ---, $10\log_{10}\left(\hat{\eta}_{21}/\eta_{21,\,ens}\right)$.

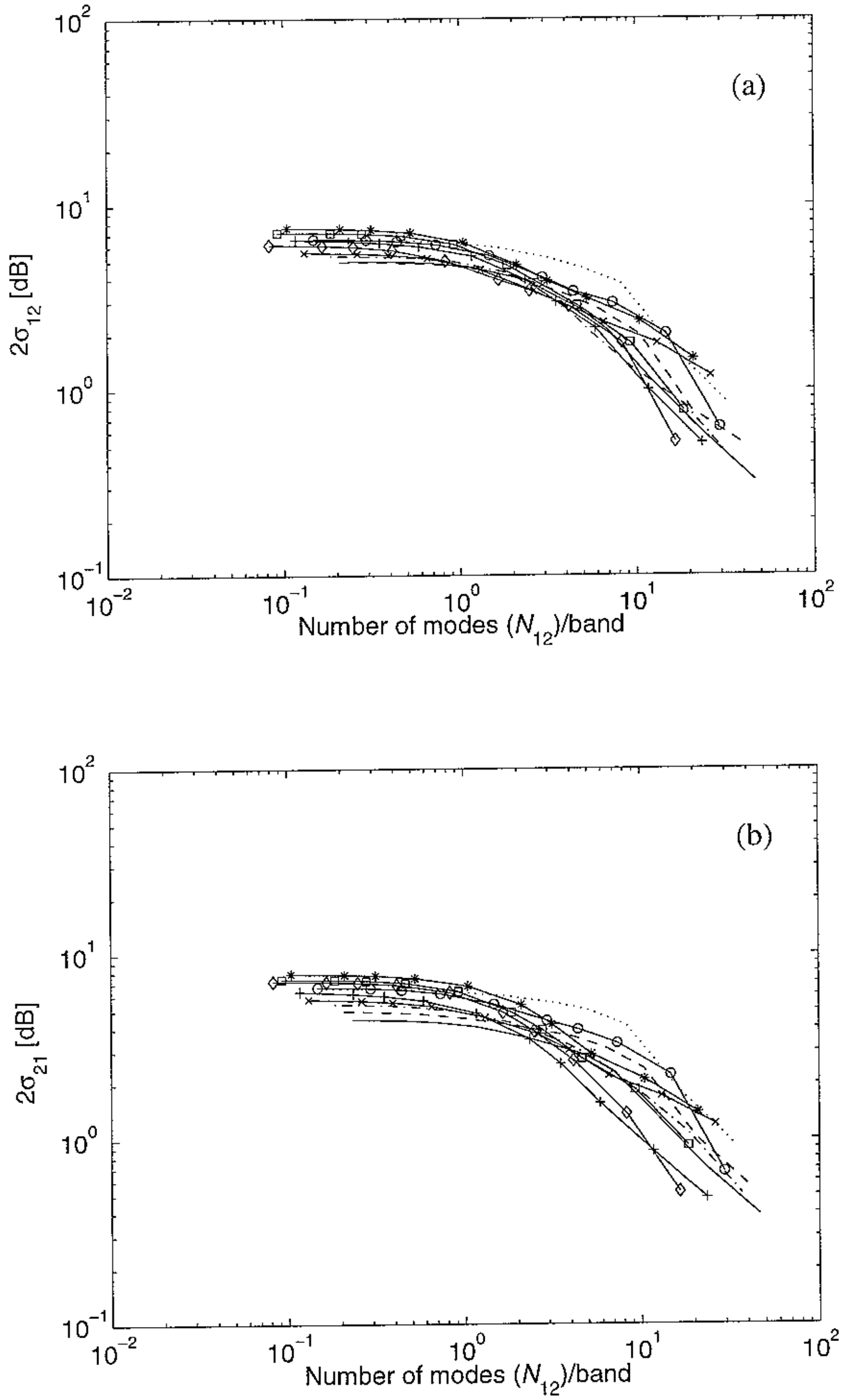

Figure 4.8. Variability of CLF (2σ), (a) σ_{12} and (b) σ_{21}, for various values of L_2. —, 1.58; ---, 1.26; -·-, 1.00; ····, 0.79; -o-, 0.63; -x-, 0.50; -+-, 0.40; -*-, 0.32; -□-, 0.25; -◇-, 0.20 (L_2 in metres).

4.4 The variation of length/width ratio (L_1/b): constant modal overlap factors without varying modal density

The influence of the plate length/width ratio L_1/b on the variability of the CLF was investigated by setting the widths of the two plates to 10 logarithmically spaced values between 0.4 and 3.16 times the original length of plate 1 ($L_1 = 0.5$m), see Table 4.3. The modal densities for the two plates were kept constant, by varying their lengths in order to keep the area and hence the modal density fixed. The damping values of the two plates were also made frequency dependent, as before in order to give constant modal overlap factors. The other parameters were the same as the baseline model. The effective CLF and the ensemble average CLF for these 10 cases were calculated and their logarithmic ratio, $10\log_{10}\left(\hat{\eta}_{ij}/\eta_{ij,\,ens}\right)$, in dB is shown in Figure 4.9, for results calculated at 1Hz spacing up to 1kHz. The results below 1.25 times the lower of the first cut-on frequencies of the two plates were also excluded, as before. Most of the CLF ratios fluctuated within ±10dB.

The results were also determined using energies averaged over frequency bands (2, 4, 6, 10, 20, 40, 60, 100, 200, and 400Hz) in overlapping bands. The two standard deviation range (2σ) for the logarithmic ratio of the frequency averaged effective CLF to the ensemble average $10\log_{10}\left(\langle\hat{\eta}_{ij}\rangle/\eta_{ij,\,ens}\right)$ was calculated in each case and 2σ is shown plotted against N_{12} in Figure 4.10. These results show that while the results are largely independent of b at low values of N_{12}, as the bandwidth is increased considerable variations occur. Especially, if the plates are narrow and long (□, ◊ in Figure 4.10), the variability of the CLF is significant even for large values of N_{12}.

Table 4.3. Parameter variations of the plate length / width ratio L_1/b for 10 variants

Parameter	h_1 (mm)	h_2 (mm)	L_1 (m)	L_2 (m)	b (m)	$n_1(\omega)$	$n_2(\omega)$	M_1	M_2
1	3.00	2.00	0.32	0.63	1.58	0.009	0.026	0.53	1.60
2	3.00	2.00	0.40	0.79	1.26	0.009	0.026	0.53	1.60
3	3.00	2.00	0.50	1.00	1.00	0.009	0.026	0.53	1.60
4	3.00	2.00	0.63	1.27	0.79	0.009	0.026	0.53	1.60
5	3.00	2.00	0.79	1.59	0.63	0.009	0.026	0.53	1.60
6	3.00	2.00	1.00	2.00	0.50	0.009	0.026	0.53	1.60
7	3.00	2.00	1.25	2.50	0.40	0.009	0.026	0.53	1.60
8	3.00	2.00	1.56	3.13	0.32	0.009	0.026	0.53	1.60
9	3.00	2.00	2.00	4.00	0.25	0.009	0.026	0.53	1.60
10	3.00	2.00	2.50	5.00	0.20	0.009	0.026	0.53	1.60

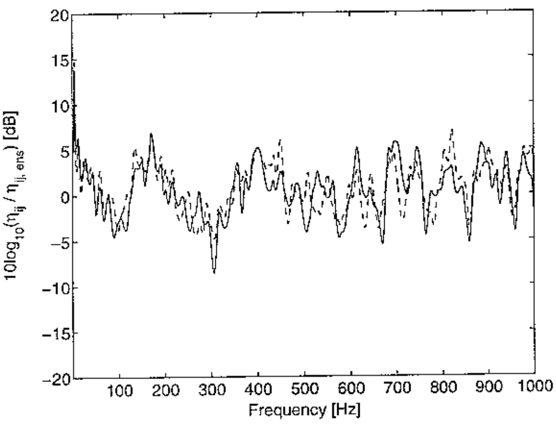

(a) $b = 1.58\text{m}$

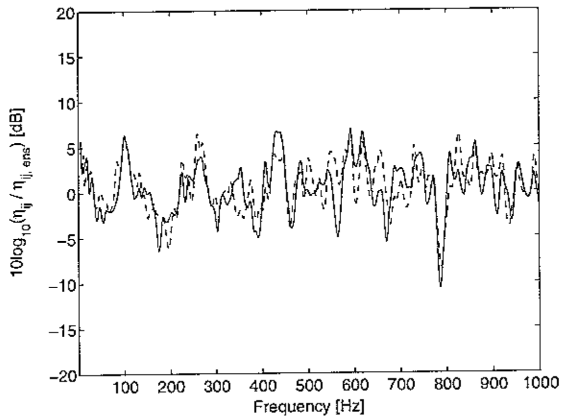

(b) $b = 1.26\text{m}$

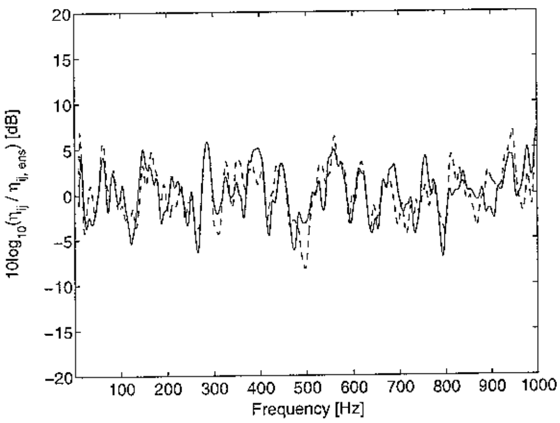

(c) $b = 1.00\text{m}$

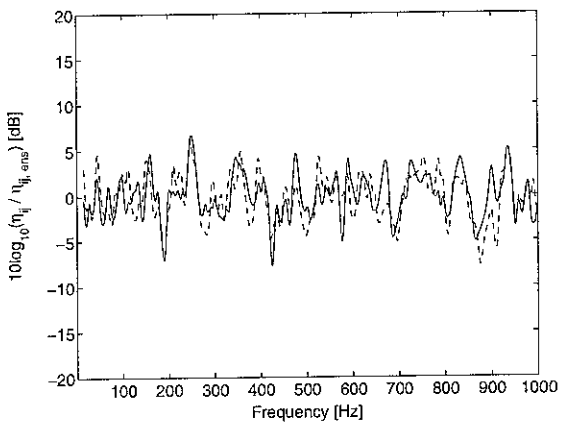

(d) $b = 0.79\text{m}$

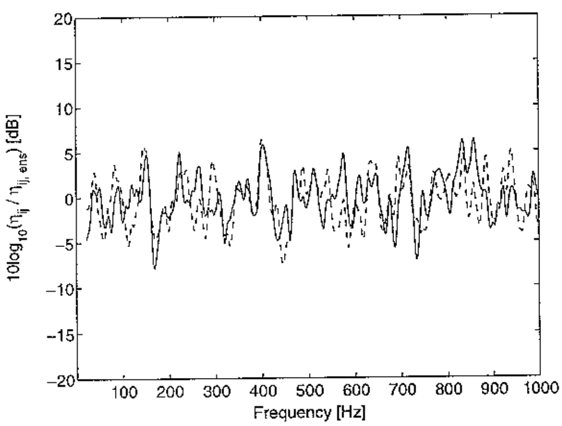

(e) $b = 0.63\text{m}$

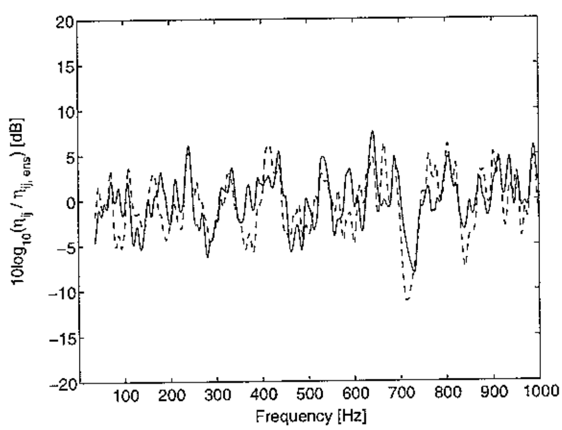

(f) $b = 0.50\text{m}$

Figure 4.9 (a)-(f). The logarithmic CLF ratio $10\log_{10}\left(\hat{\eta}_{ij}/\eta_{ij,\,ens}\right)$ for various values of b, L_1 and L_2 (area ($A_1 = 0.5\text{m}^2$, $A_2 = 1.0\ \text{m}^2$), M_1 ($= 0.53$) and M_2 ($= 1.6$) are kept constant). —, $10\log_{10}\left(\hat{\eta}_{12}/\eta_{12,\,ens}\right)$; ---, $10\log_{10}\left(\hat{\eta}_{21}/\eta_{21,\,ens}\right)$.

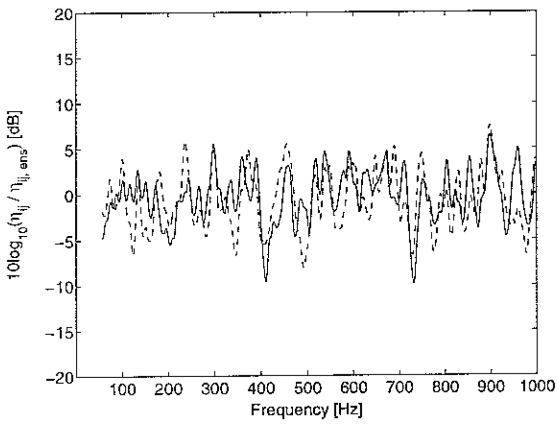

(g) $b = 0.40$m

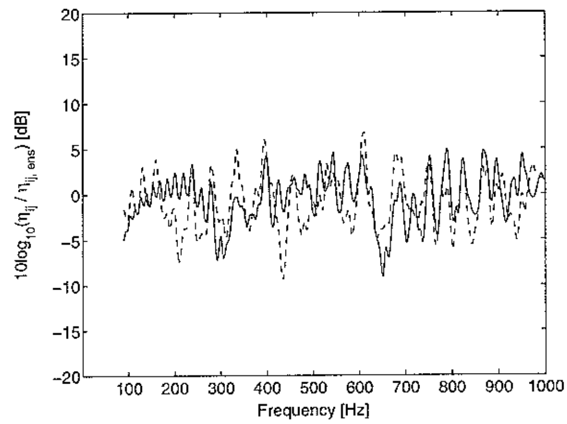

(h) $b = 0.32$m

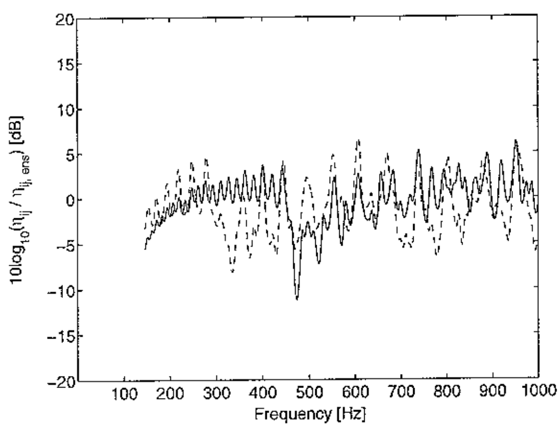

(i) $b = 0.25$m

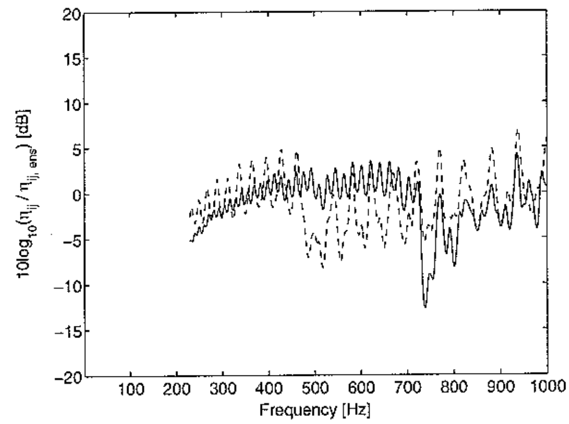

(j) $b = 0.20$m

Figure 4.9 (g)-(j). The logarithmic CLF ratio $10\log_{10}\left(\hat{\eta}_{ij}/\eta_{ij,\,ens}\right)$ for various values of b, L_1 and L_2 (area ($A_1 = 0.5\text{m}^2$, $A_2 = 1.0\ \text{m}^2$), M_1 (= 0.53) and M_2 (= 1.6) are kept constant). —, $10\log_{10}\left(\hat{\eta}_{12}/\eta_{12,\,ens}\right)$; ---, $10\log_{10}\left(\hat{\eta}_{21}/\eta_{21,\,ens}\right)$.

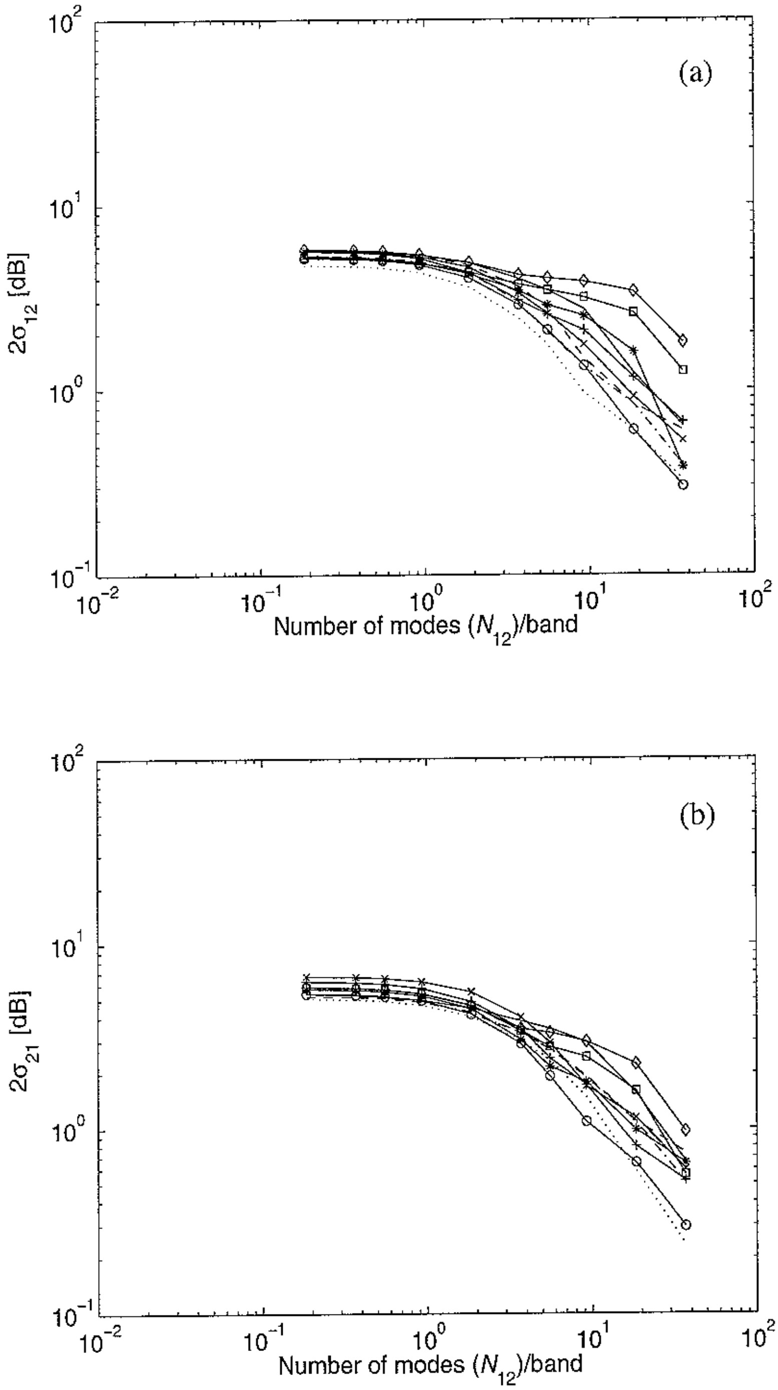

Figure 4.10. Variability of the effective CLF (2σ), (a) σ_{12} and (b) σ_{21}, for different values of b keeping plate areas and modal overlap factor constant. —, 1.58; ---, 1.26; -·-, 1.00; ····, 0.79; -o-, 0.63; -×-, 0.50; -+-, 0.40; -∗-, 0.32; -□-, 0.25; -◇-,0.20 (b in metres).

5. AN EMPIRICAL MODEL FOR THE VARIABILITY OF THE CLF

5.1 The variability of the CLF for finite plates

The results of the above extensive parameter variations are next investigated altogether to establish appropriate parameters to describe the variability of the CLF and to quantify its confidence interval. Although the results up to now have been given in terms of 2σ, it is helpful at this point to work in terms of the variance, σ^2. Firstly the results for σ^2 of the logarithmic ratio of the frequency averaged effective CLF to the ensemble averaged CLF are plotted against the number of modes per band for the source plate N_{source} or the receiver plate $N_{receiver}$, as shown in Figure 5.1(a). The results with no frequency averaging are plotted against the modal overlap factor for the source plate M_{source} or the receiver plate $M_{receiver}$, as shown in Figure 5.1(b). No clear trend can be seen from these results.

Next the results for σ^2 are plotted against $N_{12} = \sqrt{N_1 N_2}$ (the geometric mean number of modes per band), as shown in Figure 5.2(a). These results are slightly less scattered than in the previous plot, Figure 5.1. This result shows that the variability of the CLF σ^2 has a nonlinear relationship with N_{12} on log-log axes. The results for σ^2 are shown for the cases with no frequency averaging in Figure 5.2(b). These are plotted against $M_{12} = \sqrt{M_1 M_2}$ (the geometric mean modal overlap factor). These non-frequency averaged results show a linear relationship with M_{12} on log-log axes; from the slope of this relationship it is found that σ^2 is inversely proportional to M_{12}.

This can be seen to determine the constant part of the curve in Figure 5.2(a), as results for narrow frequency bands are similar to these for no frequency averaging. By multiplying all data points on Figure 5.2(a) by M_{12} the curves collapse to a similar level at low values of N_{12}. However it is also found necessary to shift the curves horizontally by a factor of $1/M_{12}$ to collapse them to a single data set.

The result is shown in Figure 5.3 in which $\sigma^2 M_{12}$ is plotted against N_{12}^2/M_{12}. A formula has been established to fit three curves to the data in Figure 5.3: $\sigma^2 M_{12} = \dfrac{a}{1 + bN_{12}^2 / M_{12}}$.

Dividing through by M_{12} these can be expressed in the form

$$\sigma^2 = \frac{a}{M_{12} + bN_{12}^2} \tag{5.1}$$

where a and b are constants for three curves. The first and third curves are fitted as the minima and maxima of the ordinate value $\sigma^2 M_{12}$ as a function of N_{12}^2/M_{12}. The values of a and b are listed in Table 5.1.

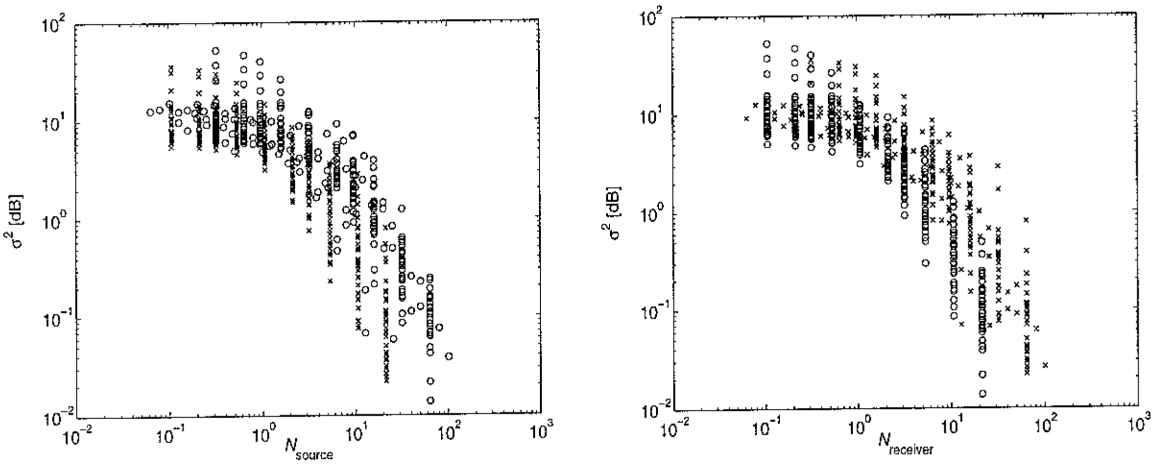

(a)

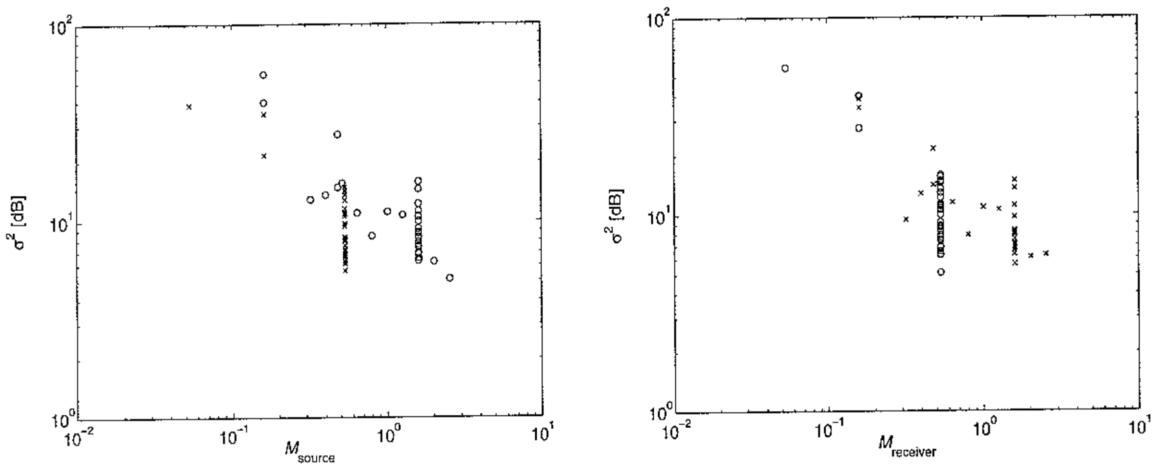

(b)

Figure 5.1. σ^2 of $10\log_{10}\left(\langle\hat{\eta}_{ij}\rangle/\eta_{ens}\right)$ for all sets of data plotted against (a) N_{source} and $N_{receiver}$ when the effective CLFs are averaged over frequency bands (2, 4, 6, 10, 20, 40, 60, 100, 200, and 400Hz) and (b) M_{source} and $M_{receiver}$ when no frequency averaging is performed. Crosses denote results for η_{12} and circles denote those for η_{21}.

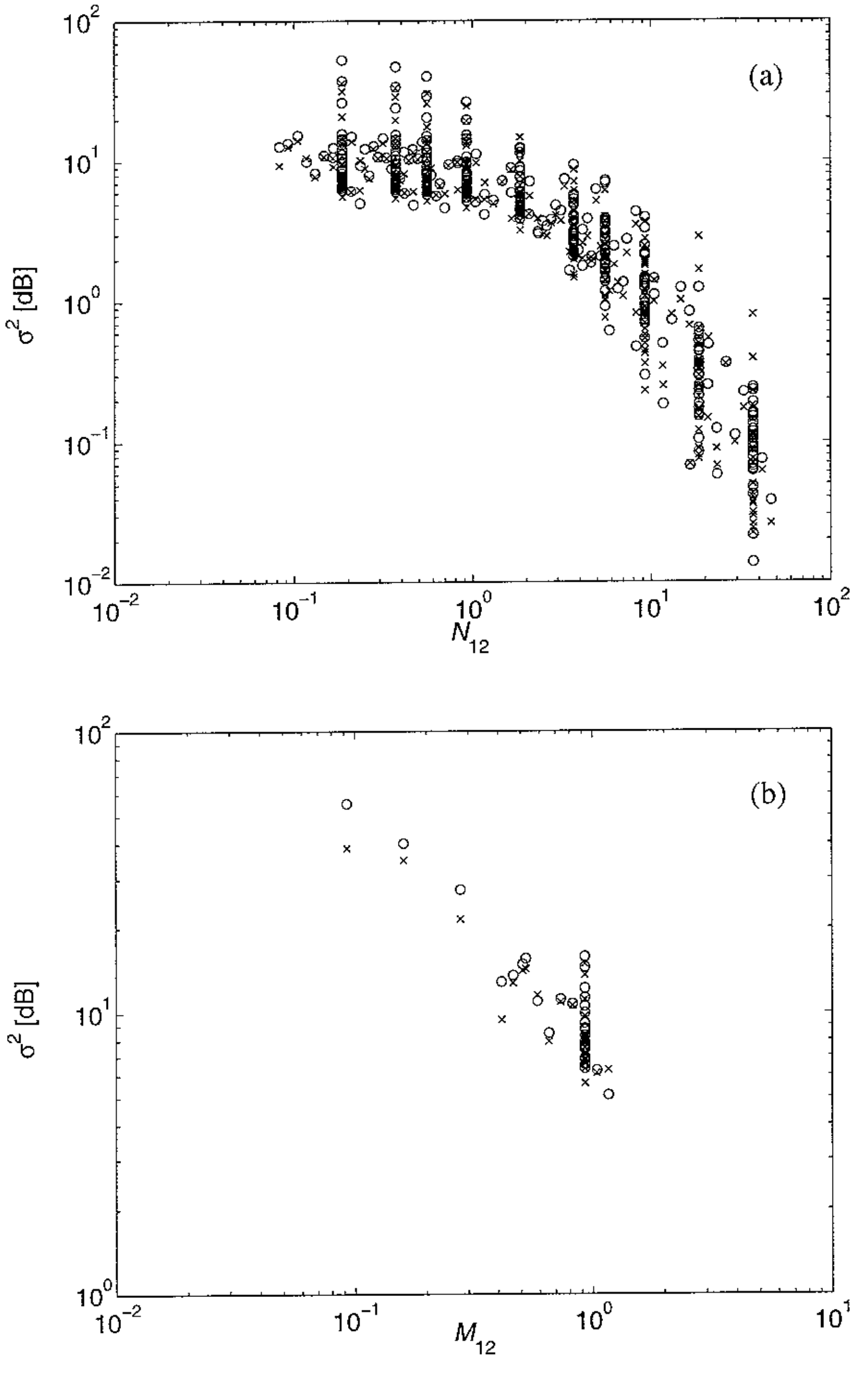

Figure 5.2. σ^2 of $10\log_{10}\left(\langle\hat{\eta}_{ij}\rangle/\eta_{ens}\right)$ for all sets of data plotted against (a) N_{12} when the effective CLFs are averaged over frequency bands (2, 4, 6, 10, 20, 40, 60, 100, 200, and 400Hz) and (b) M_{12} when no frequency averaging is performed. Crosses denote results for η_{12} and circles denote those for η_{21}.

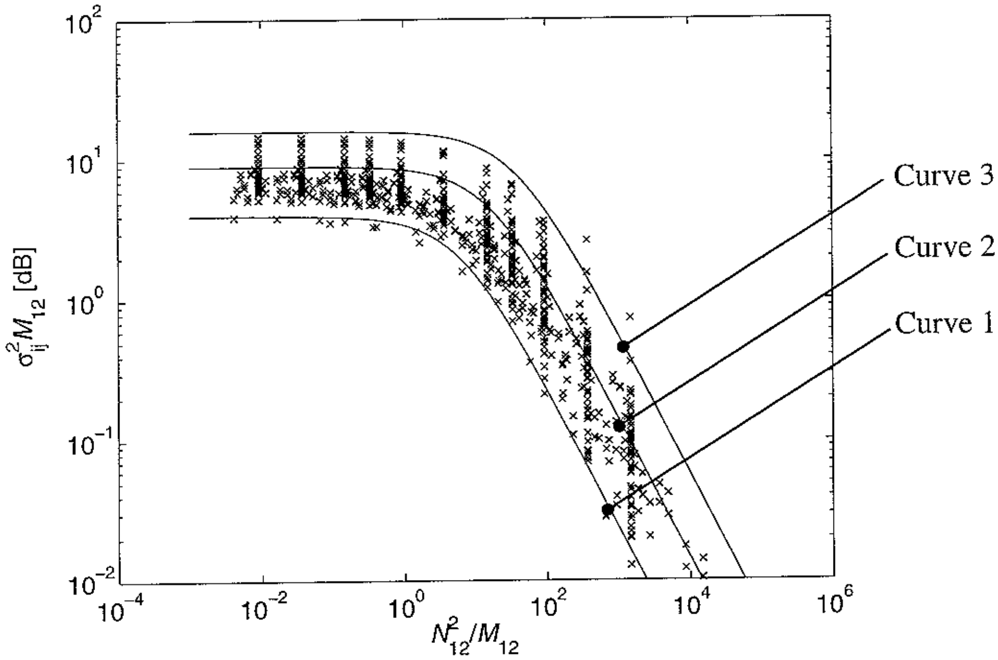

Figure 5.3. $\sigma^2 M_{12}$ plotted against N_{12}^2/M_{12} and three curves produced to quantify the variability of the CLF.

Using each of these curves rather than the original data points, a predicted confidence interval ($\pm 2\sigma$) for $10\log_{10}\left(\langle\hat{\eta}\rangle/\eta_{ens}\right)$ is determined for each pair of plates represented. In each case the percentage of frequency points falling inside this interval has been determined. Taking the average over all plates considered, it was found what confidence level each of the formulae represented. These are listed in Table 5.1. Of these, the second curve represents a 97.2% confidence interval for all sets of data and appears a suitable model.

Table 5.1 Percentage of points falling within $\pm 2\sigma$ limits defined by $\sigma^2 = \dfrac{a}{M_{12} + bN_{12}^2}$ for all sets of data.

Curve	a	b	Confidence interval (%)
1	4	1/6	82.3
2	9	1/16	97.2
3	16	1/36	99.7

5.2 New parameters for finite-infinite plates

In order to apply the above concepts to the results for a finite plate coupled to an infinite plate or an infinite plate coupled to a finite plate, the two parameters, M_{12} and N_{12}, cannot be used since the number of modes and modal densities for an infinite plate tend to infinity. The CLF ratio for a model with an infinite receiver plate from [11] and upper and lower bounds obtained from equation (5.1) using $2M_1$ and $2N_1$ are shown in Figure 5.4(a). Figure 5.4(b) shows the results of an infinite plate coupled to a finite plate for $n = 1$ along with bounds obtained from $2N_2$ and $2M_2$. These give a reasonable upper and lower bounds for the CLF for those models. Therefore, instead of M_{12} and N_{12}, new parameters M_{comb} and N_{comb}, are proposed, given by

$$M_{\text{comb}} = \frac{2M_1M_2}{M_1+M_2}. \tag{5.2}$$

It may be noted that $M_{\text{comb}} \approx M_{12}$ for $M_1 \sim M_2$, $M_{\text{comb}} = 2M_1$ for $M_2 \to \infty$, and $M_{\text{comb}} = 2M_2$ for $M_1 \to \infty$. Similarly

$$N_{\text{comb}} = \frac{2N_1N_2}{N_1+N_2} \tag{5.3}$$

which satisfies $N_{\text{comb}} \approx N_{12}$ for $N_1 \sim N_2$, $N_{\text{comb}} = 2N_1$ for $N_2 \to \infty$, and $N_{\text{comb}} = 2N_2$ for $N_1 \to \infty$. Equations (5.2) and (5.3) are based on the following relationship; $\frac{1}{M_{\text{comb}}} = \frac{1}{2}\left(\frac{1}{M_1}+\frac{1}{M_2}\right)$ and $\frac{1}{N_{\text{comb}}} = \frac{1}{2}\left(\frac{1}{N_1}+\frac{1}{N_2}\right)$, and reflect the fact that the smaller N or M dominates the variability of the CLF most. Figure (5.5) shows N_{comb}/N_1 and N_{comb}/N_2 plotted against N_2/N_1. These are compared with N_{12}/N_1 and N_{12}/N_2. This plot shows that two values are close when $N_1 \sim N_2$. The values of N_2/N_1 and M_2/M_1 considered in the parameter variations in section 4 are limited to the range 0.6 to 4.74.

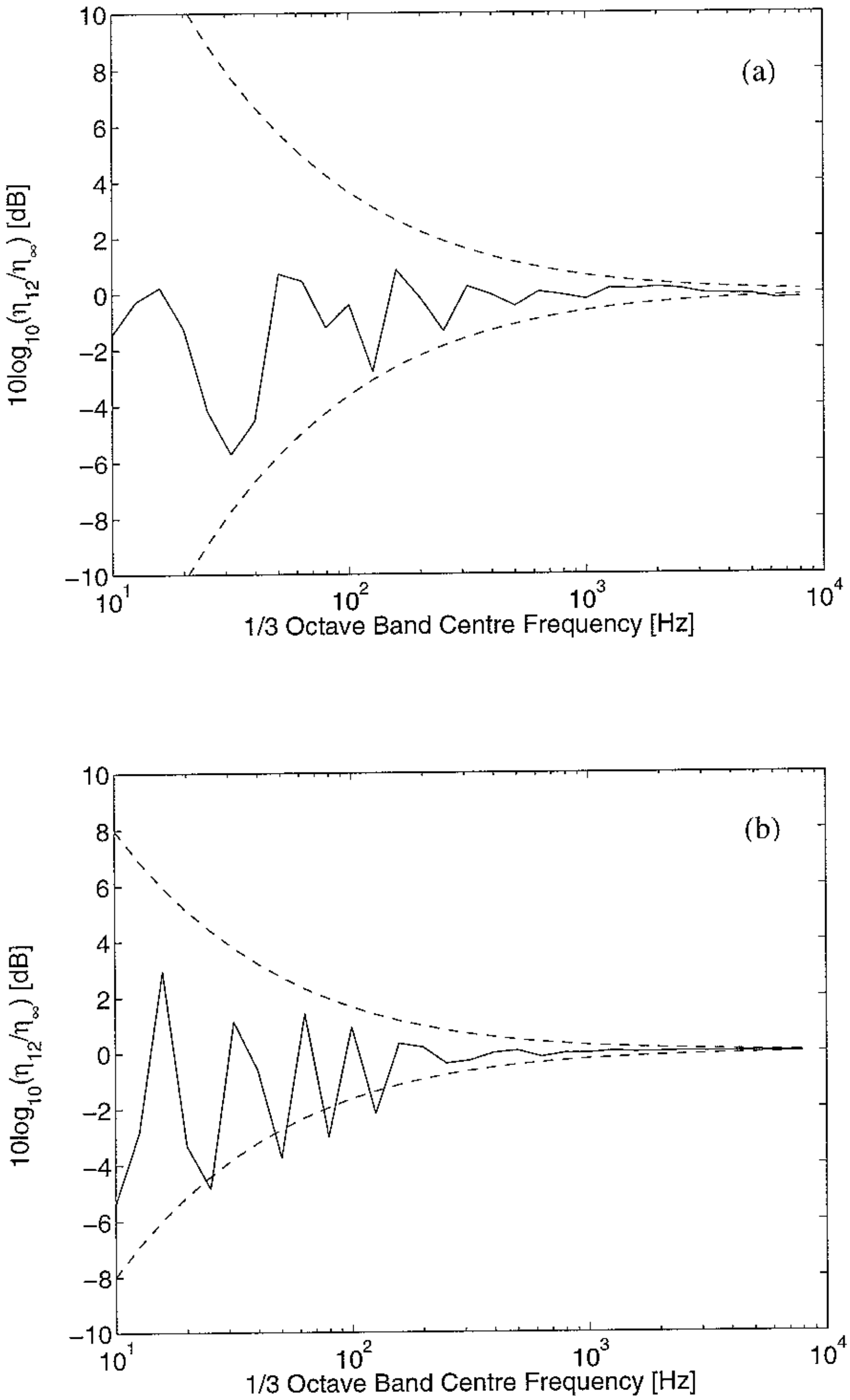

Figure 5.4. The effective CLFs and upper and lower bounds for (a) a finite plate coupled to an infinite plate and (b) an infinite plate coupled to a finite plate for $n = 1$. —, $10\log_{10}\left(\hat{\eta}_{12}/\eta_{12,ens}\right)$; ---, upper and lower bounds obtained from equation (5.1) using $2M_1$ and $2N_1$ or $2M_2$ and $2N_2$ instead of M_{12} and N_{12}.

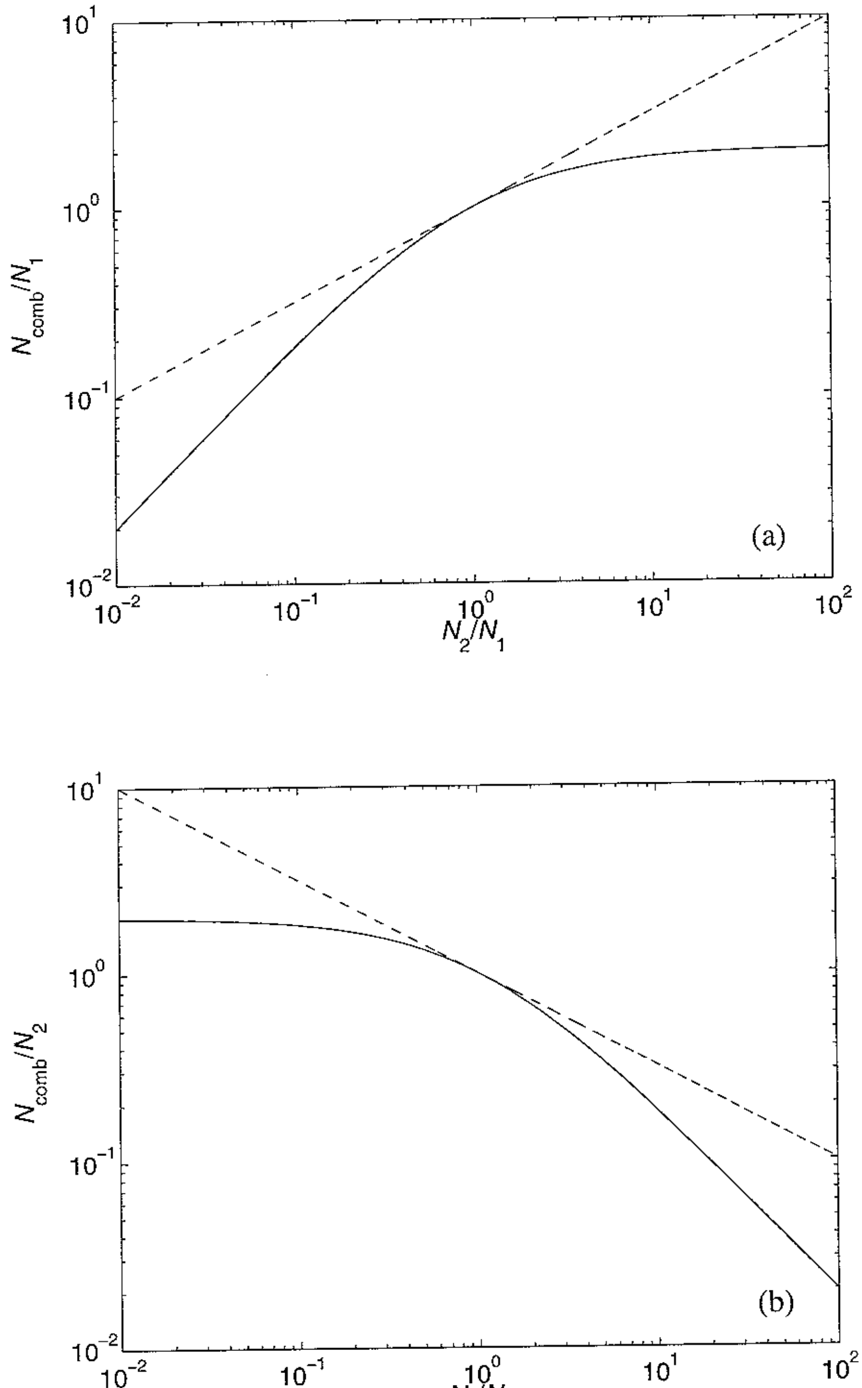

Figure 5.5. N_{comb}/N and N_{12}/N plotted against N_2/N_1. (a) —, N_{comb}/N_1; ---, N_{12}/N_1 and (b) —, N_{comb}/N_2; ---, N_{12}/N_2

5.3 The derivation of an empirical model

Using the same method as section 5.1, a similar result is shown in Figure 5.6 in which $\sigma^2 M_{\text{comb}}$ is plotted against $N^2_{\text{comb}}/M_{\text{comb}}$. In the same way as above, a formula has been established to fit three curves to the data in Figure 5.6: $\sigma^2 M_{\text{comb}} = \dfrac{c}{1 + dN^2_{\text{comb}} / M_{\text{comb}}}$.

Dividing through by M_{comb} these can be expressed in the form

$$\sigma^2 = \frac{c}{M_{\text{comb}} + dN^2_{\text{comb}}} \tag{5.4}$$

where c and d are constants for the three curves. The confidence interval represented by each of these curves has been determined and is listed in Table 5.2. Of these, the second curve is adopted as the "empirical model" for the variability of the CLF:

$$\sigma^2 = \frac{6}{M_{\text{comb}} + N^2_{\text{comb}}/16}. \tag{5.5}$$

This represents a 95.7% confidence interval for all sets of data. This model can be generally used to evaluate the uncertainty of the CLF of a two-coupled plate system.

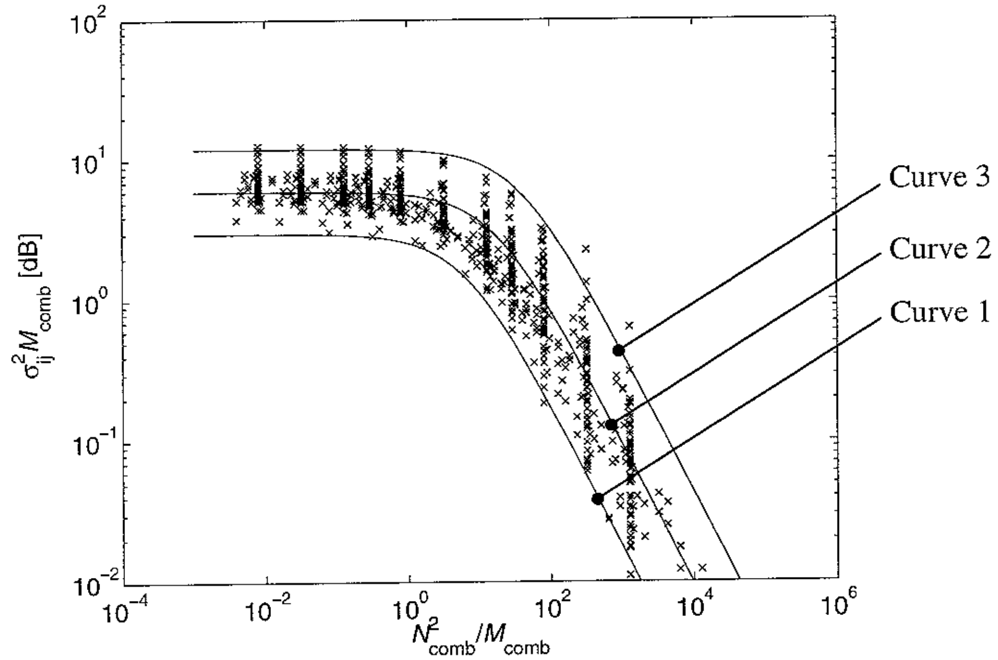

Figure 5.6. $\sigma^2 M_{comb}$ plotted against N^2_{comb}/M_{comb} and three curves produced to quantify the variability of the CLF.

Table 5.2 Percentage of points falling within $\pm 2\sigma$ limits defined by $\sigma^2 = \dfrac{c}{M_{comb} + dN^2_{comb}}$ for all sets of data.

Curve	c	d	Confidence interval (%)
1	3	1/6	80.1
2	6	1/16	95.7
3	12	1/36	99.6

5.4 Comparison with previously published model

A similar investigation for two coupled plates, for which only the plate length ratio L_1/L_2 was varied, was performed by Mohammed [14]. He suggested a semi-empirical formula,

$$\left\{\frac{\sigma^2}{\left\langle \hat{\eta}_{ij} \right\rangle^2}\right\} = \log_{10} c + 1.3\log_{10} M_{12} + 1.25\log_{10} N_{12} \tag{5.6}$$

where σ^2 is the variance of the CLF, $\left\langle \hat{\eta}_{ij} \right\rangle$ is the mean value of the CLF and c is a constant which was determined by plotting the different sets of data and performing best straight line fits on log-log axes. The current results, displayed in Figure 5.6, have been converted into the form used in Mohammed's model and are plotted in Figure 5.7. This result shows that the current results cannot be represented by a straight line as suggested by Mohammed. The present data set far exceeds the number of configurations previously used [14]. The present model therefore seems more appropriate.

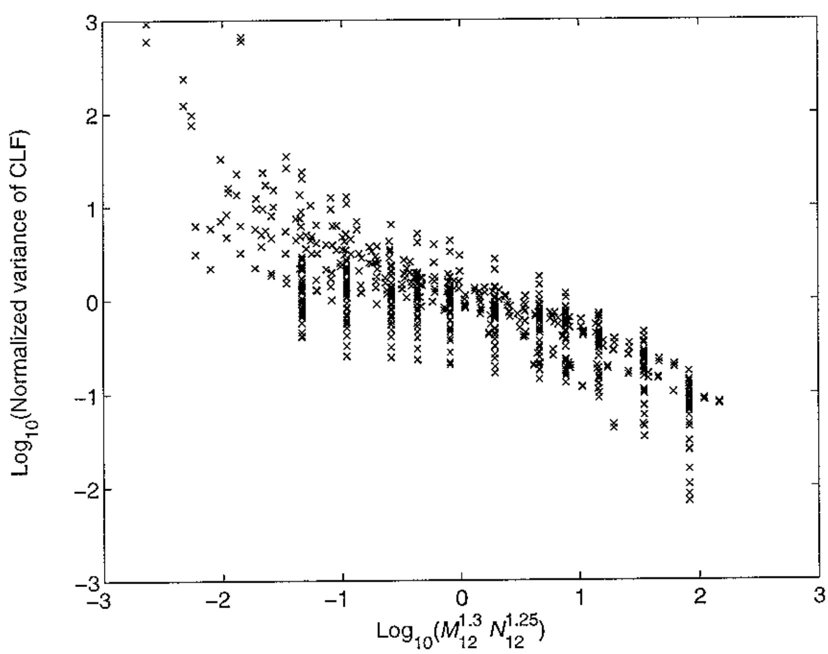

Figure 5.7. The normalised variance $\frac{\sigma^2}{\left\langle \hat{\eta}_{ij} \right\rangle}$ plotted against $(M_{12})^{1.3}(N_{12})^{1.25}$ based on the Mohammed's formula [14].

5.5 Comparison with previous calculations

The variability of the effective CLF found in the previous parameter variations [1] have been compared to the estimates based on equation (5.5). These results were in 1/3 octave bands and covered variations in thickness ratio, length ratio, and length/width ratio. The logarithmic ratio of the effective CLF to the ensemble average $10\log_{10}\left(\left\langle\hat{\eta}_{ij}\right\rangle/\eta_{ij,\,ens}\right)$ was determined and these results are shown in Figure 5.8. These $\pm 2\sigma$ estimates give better upper and lower bounds for the effective CLF than Craik's model investigated in the previous study [1]. The deviations at high frequencies in Figure 5.8(a) are due to in-plane motion included in the DSM model but not the ensemble average.

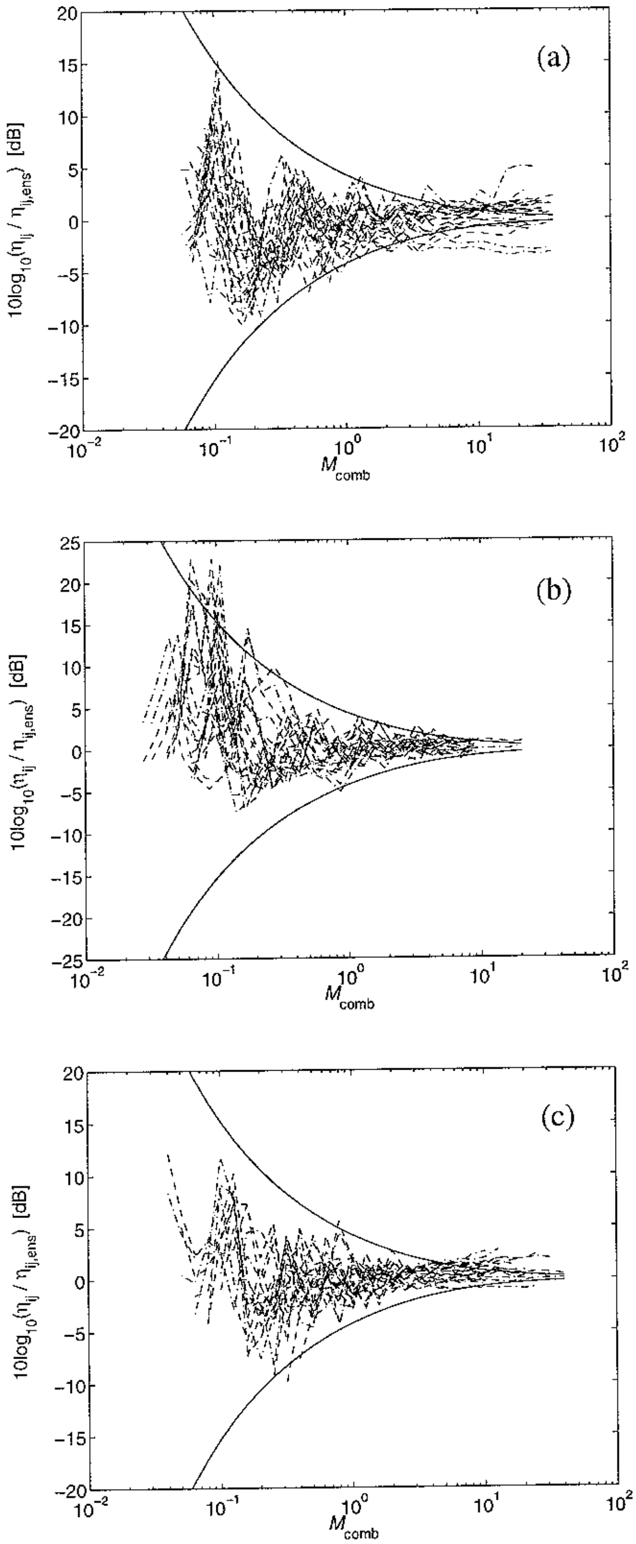

Figure 5.8. Logarithmic CLF ratio $10\log_{10}\left(\langle\hat{\eta}_{ij}\rangle/\eta_{ij,ens}\right)$ plotted against M_{comb} results in 1/3 octave bands from [1]. (a) varying thickness ratio, (b) varying length ratio, and (c) varying length/width ratio. ---, $10\log_{10}\left(\langle\hat{\eta}_{12}\rangle/\eta_{12,ens}\right)$; -·-, $10\log_{10}\left(\langle\hat{\eta}_{21}\rangle/\eta_{21,ens}\right)$; —, $\pm 2\sigma$ estimate based on equation (5.5).

6. CONCLUSIONS

In this study, the variability of the coupling loss factor (CLF) for a system of two coupled rectangular plates has been examined and quantified using a systematic parameter variation. An empirical model for the variability of the CLF has been developed using these results.

Firstly, the ensemble average CLF given by Wester and Mace [2] was used to improve the estimate of the average CLF for a case of 1/3 octave bands and a constant loss factor. At low frequencies the ensemble average CLFs are lower than the semi-infinite results $\eta_{ij\infty}$ and the effective CLFs fluctuate considerably relative to $\eta_{ij,\,ens}$. These CLFs all coincide closely at high frequency. The influence of damping on the ensemble average CLF was also investigated.

Secondly, narrow band energies and powers were calculated for a large number of configurations using the dynamic stiffness method. The modal overlap factor was kept constant versus frequency by using a loss factor inversely proportional to frequency. The effective CLFs averaged over frequency bands $\langle \hat{\eta}_{ij} \rangle$ were obtained from these energies. The effects of frequency and modal overlap were separated by using frequency averages at a series of constant bandwidths rather than 1/3 octave averages.

Finally, the logarithmic ratio of the effective CLF to the ensemble average, $10\log_{10}\left(\langle \hat{\eta}_{ij} \rangle / \eta_{ij,\,ens}\right)$, was determined and the variance σ^2 was obtained over the whole frequency region to express the variability of the effective CLF compared to the ensemble average. An empirical model was developed to express the dependence of the variance σ^2 on the modal overlap factors and numbers of modes in a frequency band. This is given by $\sigma^2 = \dfrac{6}{M_{\mathrm{comb}} + N_{\mathrm{comb}}^2/16}$ where $M_{\mathrm{comb}} = \dfrac{2M_1M_2}{M_1+N_2}$ and $N_{\mathrm{comb}} = \dfrac{2N_1N_2}{N_1+N_2}$.

This represents a 95.7% confidence interval for all sets of data considered. This model was developed for two coupled rectangular plate system and can be used to evaluate the uncertainty of the CLF of that system. However it is not known whether other types of system can be represented by the same model.

REFERENCES

[1] W. S. Park, D. J. Thompson and N. S. Ferguson 2000 *ISVR Technical Memorandum* No.856, Sources of error and confidence intervals for SEA parameters of two coupled rectangular plates.

[2] E. C. N. Wester and B. R. Mace 1996 *Journal of Sound and Vibration* **193**(4), 793-822. Statistical energy analysis of two edge-coupled rectangular plates: Ensemble averages.

[3] R. J. M. Craik, J. A. Steel and D. I. Evans 1991 *Journal of Sound and Vibration* **144**(1), 95-107. Statistical energy analysis of structure-borne sound transmission at low frequencies.

[4] J. A. Steel and R. J. M. Craik 1994 *Journal of Sound and Vibration* **178**(4), 553-561. Statistical energy analysis of structure-borne sound transmission by finite element methods.

[5] H. G. Davies and M. A. Wahab 1981 *Journal of Sound and Vibration* **77**(3), 311-321. Ensemble average of power flow in randomly excited coupled beams.

[6] B. R. Mace 1993 *Journal of Sound and Vibration* **166**(3), 429-461. The statistical energy analysis of two continuous one-dimensional subsystems.

[7] B. R. Mace 1996 *Journal of Sound and Vibration* **189**(4), 443-476. Finite frequency band averaging effects in the statistical energy analysis of two continuous one-dimensional subsystems.

[8] F. Fahy 1997 in *Statistical Energy Analysis; An overview, with applications in structural dynamics* (A. J. Keane and W. G. Price, editors), Cambridge University Press. Statistical energy analysis: A critical overview.

[9] L. Cremer, M. Heckl and E. E. Ungar 1988 *Structure-borne Sound: Structural Vibrations and Sound Radiation at Audio Frequencies.* New York: Springer-Verlag; second edition.

[10] R. H. Lyon and R. G. DeJong 1995 *Theory and Application of Statistical Energy Analysis.* Boston, Massachusetts: Butterworth-Heinemann; second edition.

[11] W. S. Park, D. J. Thompson and N. S. Ferguson 2001 *ISVR Technical Memorandum* No.861, The influence of the source and receiver modal behaviour on power transmission between two subsystems.

[12] S. Timishenko and S. Woinowsky-Krieger 1959 *Theory of Plates and Shells.* New York: McGraw-Hill; second edition.

[13] E. Skudrzyk 1980 *Journal of the Acoustical Society of America* **67**(4) 1105-1135. The mean-value method of predicting the dynamic response of complex vibrations.

[14] A. D. Mohammed 1990 *Ph.D. Thesis, University of Southampton.* A study of uncertainty in applications of Statistical Energy Analysis.